
PERGAMON

Progress in Energy and Combustion Science 28 (2002) 435–475

PROGRESS IN ENERGY AND COMBUSTION SCIENCE

www.elsevier.com/locate/pecs

Edge-flames

J. Buckmaster*

Department of Aeronautical and Astronautical Engineering, University of Illinois at Urbana-Champaign, 104 S. Wright Street, Urbana, IL 61801, USA

Received 5 November 2001; accepted 17 July 2002

Abstract

This review discusses the essential nature of edge-flames, how they are defined, the nature of their structure, how it is that both positive and negative edge-speeds can arise. Their roots in mixing-layer flames are extensively described, but premixed edge-flames are also discussed, rooted in the multivalued 1D solutions that can be exhibited by certain kinds of deflagrations. Cellular instabilities of both non-premixed and premixed edge-flames located in counterflows are examined, and links with flame-strings and flame-balls are discussed when one or more Lewis numbers are small. And the pulsating instability commonly associated with large Lewis numbers is examined in a simple model context that has some of the characteristics of experimentally realizable flames, such as the microgravity candle flame. Lifted edge-flames, both laminar and turbulent are described, as are some aspects of non-premixed edge-flame holding. © 2002 Elsevier Science Ltd. All rights reserved.

Keywords: Edge-flames; Laminar flames; Premixed combustion; Non-premixed combustion; Flame-holding; Flame stability; Lifted flames; Holes in flames

Contents

* Tel.: +1-217-333-1803; fax: +1-217-244-0720.
E-mail address: limey@uiuc.edu (J. Buckmaster).

0360-1285/02/$ - see front matter © 2002 Elsevier Science Ltd. All rights reserved.
PII: S0360-1285(02)00008-4

1. Introduction

There are two one-dimensional (1D) flame structures at the heart of any discussion of flame physics—the plane deflagration, and the 1D diffusion flame as realized, for example, in the counterflow configuration. We study 1D flames for their universal character, for the physical insights so obtained, for a vocabulary, all relevant to a large number of flame configurations. Likewise, edge-flames are idealized two-dimensional (2D) structures that provide an intellectual framework of universal significance, and help us to understand flames with edges.

Flames with edges occur in many forms, and several examples are sketched in Fig. 1. Fig. 1a shows a flame spreading over a fuel-bed, solid or liquid. Most of the fuel flux (non-uniform) from the bed is consumed in a diffusion flame that is nominally 1D (1̃D), but reaction is negligible at the temperature of the bed surface so that there is a dead space between the flame and the bed, and the flame has an edge [1].

Fig. 1b shows a candle-flame burning under microgravity conditions. (Candle-burning experiments have been carried out on both the Space-shuttle and the Mir space station [2].) In the absence of buoyancy-induced currents, the flame is roughly hemispherical in shape, with a well-defined circular edge. This edge is usually stationary, but prior to extinction it oscillates up and down, an issue that we shall discuss in some detail.

Fig. 1c is an idealization of a portion of the combustion field supported by a heterogeneous propellant of the kind used in rocket motors. Shown is a diffusion flame in which the fuel (binder) and oxidizer (ammonium perchlorate decomposition products) react, and this flame has an edge [3]. Reaction at the edge is stronger than in the trailing 1̃D diffusion flame, and generates heat that plays a key role in the regression of the propellant surface [4].

Fig. 1d shows a diffusion flame distorted by turbulence. Quenching occurs at those times and those places where the scalar dissipation rate (a stochastic variable) is large enough, and in this way holes are formed in the flame [5]. Each hole has an edge, also an edge for the surrounding 1̃D flame.

Fig. 1e shows a sequence of pictures obtained in experiments reported by Jarosinski and co-authors in 1982 [6]. A *sublimit* lean methane/air flame (premixed) rises up a standard inflammability tube, and after a short time begins to fail. Failure starts with the appearance of a small hole at the flame tip (frame 13), and the hole expands. Failure is complete when the flame edge has retreated completely down the flame skirt.

Fig. 1f shows an axisymmetric diffusion flame supported on a tube burner, burning under microgravity conditions [7]. There is an edge near the burner rim, similar to that of Fig. 1c, and in addition there is an edge near the tip, since the tip is open, a consequence perhaps of radiation cooling.

And Fig. 1g shows an experimental configuration studied in Refs. [8,9] which has some similarities to the flame spread configuration (Fig. 1a). Air is passed over a plate through which fuel is injected, and in this way a reactive boundary layer is formed in which is located a 1̃D diffusion flame with an edge.

As a final example (but a configuration we do not draw), the flame supported by a fuel plate in an airflow is discussed in Ref. [10]. At large Damköhler numbers the flame envelops the front of the plate (closed tip); but at small Damköhler numbers the tip is open so that there are well-defined flame edges at the top and bottom plate surfaces.

In due course we shall describe idealized edge-flames which are paradigms for these various flames with edges; classical 1D flames provide some of the building blocks of these structures. Unbounded edge-flames exhibit wave-like behavior (Fig. 1a and b), as do 1D deflagrations, and the concept of edge-speed is as meaningful as the concept of flame-speed. (And for anchored edge-flames (Fig. 1c), the concept of edge-speed is as problematic as the concept of flame-speed is for anchored deflagrations). There are connections then between edge-flames and 1D flames, and because of this we shall start with a brief discussion of the latter.

2. Deflagrations and the concept of flame-speed

There is much wishful thinking in the discussion of flame-speed in the literature (and this author has thought his share), justification for a few remarks about this old subject.

It is sufficient for our purposes to examine the concept in

Nomenclature

B	pre-exponential constant in reaction rate
$\mathscr{D}$, $\mathscr{D}_i$	mass diffusion coefficient
D	Damköhler number
D_0	value of D for which the edge-speed is zero
D_1	$\varepsilon^3 D(1-\theta_w)^{-1}$
D_e	1D extinction value of D
D_i	1D ignition value of D
E	activation energy
L	characteristic geometric length
n	coordinate normal to flame-sheet
Q	heat of reaction
R	universal gas constant
S_o	adiabatic flame-speed
T	temperature
T_{ad}	adiabatic flame-temperature
T_{G_s}	Burke–Schumann flame temperature
U	dimensional edge- or wave-speed
V	dimensionless edge- or wave-speed
x	coordinate perpendicular to edge-flame travel
X	mass fraction of oxidizer
Y	mass fraction of fuel
z	coordinate parallel to edge-flame travel
$(\cdot)_w$	wall values
$(\cdot)_*$	flame conditions
$(\cdot)_f$	fresh mixture supply
$(\cdot)_\infty$	supply conditions
α	rate of strain
$\alpha_{X,Y}$	stoichiometric coefficients
ε	inverse activation energy
ϕ	equivalence ratio, temperature perturbation
Φ	Schvab–Zeldovich variable
γ_m	Markstein number
ρ	density
θ	temperature

the context of the equations

$$\rho C_p\left(\frac{\partial T}{\partial t}+\mathbf{q}\cdot\nabla T\right)=\lambda\nabla^2 T+QBY\,\mathrm{e}^{-E/RT},$$
$$\rho\left(\frac{\partial Y}{\partial t}+\mathbf{q}\cdot\nabla Y\right)=\rho\mathscr{D}\nabla^2 Y-BY\,\mathrm{e}^{-E/RT}, \tag{1}$$

where $\mathbf{q}$ is either an assigned solenoidal velocity field (as for the constant-density model) or is to be simultaneously determined from the Navier–Stokes equations. We shall discuss the solutions of Eqs. (1) in the limit $E\to\infty$.

The standard approach is to restrict attention to the class of problems for which the flame-temperature (the temperature at the vanishingly thin reaction zone or flame-sheet) varies both in time and space by only asymptotically small amounts, and the temperature gradient on the burnt-gas side of the sheet is asymptotically small. Reaction is then zero in the burnt gas because $Y\equiv 0$ there, and not because of reaction freezing. On the scale of the preheat zone the sheet is vanishingly thin, and its normal, directed towards the burnt gas, is to first order well defined. If n is the distance measured along this normal, the flame-sheet structure is defined by a diffusion-reaction balance, viz.

$$0=\lambda\frac{\partial^2 T}{\partial n^2}+QBY\,\mathrm{e}^{-E/RT},$$
$$0=\rho\mathscr{D}\frac{\partial^2 Y}{\partial n^2}-BY\,\mathrm{e}^{-E/RT}. \tag{2}$$

In the usual way, we seek a solution by writing

$$T=T_*+\varepsilon t(\eta),\qquad Y=\varepsilon y(\eta),\qquad n=\varepsilon\eta,$$
$$\varepsilon=\frac{RT_*}{E}\to 0, \tag{3}$$

whence

$$-\frac{\lambda}{Q}\frac{\mathrm{d}^2 t}{\mathrm{d}\eta^2}=\rho\mathscr{D}\frac{\mathrm{d}^2 y}{\mathrm{d}\eta^2}=\varepsilon^2\,\mathrm{e}^{-1/\varepsilon}By\,\mathrm{e}^{t/T_*}. \tag{4}$$

Here T_* is the flame-temperature, the temperature at $\eta\to\infty$ where, in addition, $Y\to 0$. Therefore, on integrating Eq. (4) twice,

$$\frac{\lambda}{Q}t+\rho\mathscr{D}y=0. \tag{5}$$

The equation for t defined by Eqs. (4) and (5) can be integrated once to yield

$$\left(\frac{\mathrm{d}t}{\mathrm{d}\eta}\right)^2=\frac{2\varepsilon^2\,\mathrm{e}^{-1/\varepsilon}B}{\rho\mathscr{D}}[T_* t\,\mathrm{e}^{t/T_*}-T_*^2\,\mathrm{e}^{t/T_*}+T_*^2] \tag{6}$$

($\mathrm{d}t/\mathrm{d}\eta=0$ when $t=0$, $\eta\to\infty$) whence the Y-gradient on the upstream side of the sheet ($\eta\to-\infty$, $t\to-\infty$) is

$$-\rho\mathscr{D}\frac{\mathrm{d}Y}{\mathrm{d}n_-}=\frac{\lambda}{Q}\sqrt{\frac{2B}{\rho\mathscr{D}}}\frac{T_*^2 R}{E}\mathrm{e}^{-E/2RT_*}. \tag{7}$$

In the context of the model described by Eqs. (1), this familiar result is the central one from which the essential behavior of deflagrations flows. Fundamentally it says that the flux of the reactant Y to the flame-sheet, all of which is consumed there, is an Arrhenius function of the flame-temperature. Thus the flame-temperature and the reactant flux are measures of the strength of the flame, and these measures arise in a natural and direct fashion without reference to flame-speed.

The flame-sheet must position itself or move so that condition (7) is satisfied. For a plane steady unbounded deflagration ($\partial/\partial t=0$, $\rho\mathbf{q}\cdot\nabla\to M(\partial/\partial n)$) conservation of the flux of Y within the preheat zone means that

$$-\rho\mathscr{D}\frac{\partial Y}{\partial n_-}=MY_\infty \tag{8}$$

where Y_∞ is a supply value, and this determines the flame-speed M/ρ_∞ in terms of the flame-temperature. When the

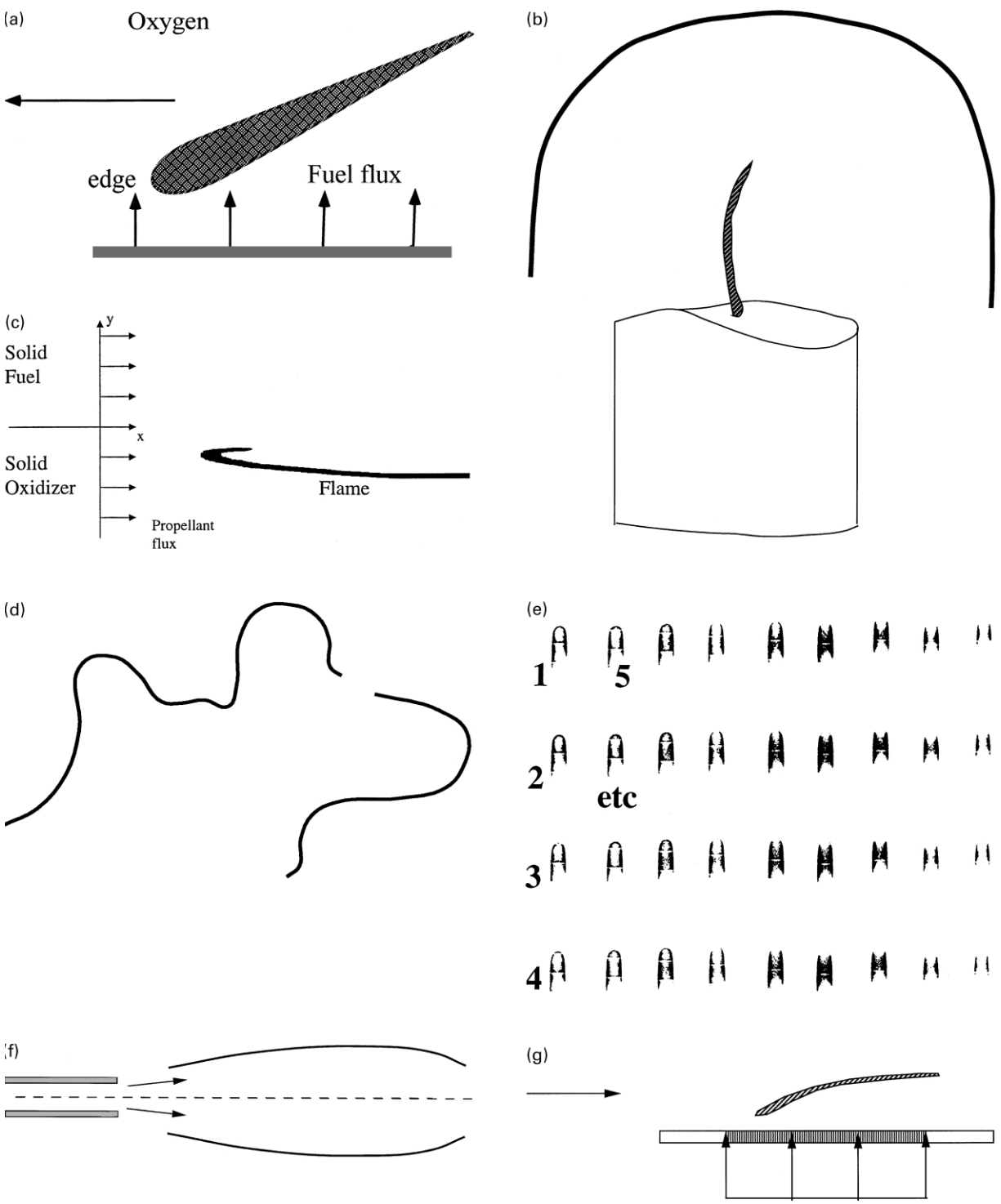

Fig. 1. (a) Flame spreading over a fuel-bed. (b) Candle flame burning under microgravity conditions. (c) A diffusion flame with an edge supported by fluxes from a heterogeneous propellant. (d) A wrinkled torn flame in a turbulent flow. (e) A sequence of pictures of a sublimit methane/air flame traveling up a standard inflammability tube, from Ref. [6], with permission. (f) An axisymmetric diffusion flame under microgravity conditions [7]. (g) A diffusion flame sitting on a plate through which fuel is injected [8,9].

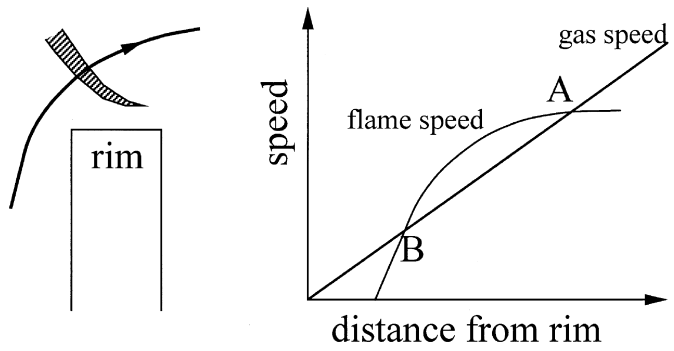

Fig. 2. A deflagration anchored to a burner rim [14], and variations in gas-speed and flame-speed from which stability conclusions are drawn. The left panel shows a streamline along which the gas speed increases, as shown in the right panel. The flame-speed increases with distance from the rim as the cooling effect decreases, asymptoting to the adiabatic flame-speed.

latter is determined from energy considerations, the flame-speed is determined.

More generally, flame-speed is well defined in the hydrodynamic limit $Pe_L \to \infty$, where $Pe_L = MC_pL/\lambda$ is the Peclet number based on L, a length characteristic of the flame geometry.

Difficulties arise as soon as one moves away from the limit. Thus consider Markstein's famous flame-speed correction, proposed in the context of weakly stretched flames, and addressed by Markstein solely in the context of the flame as a hydrodynamic discontinuity [11]. Suppose, for example, the flame is placed in a non-uniform velocity field which is locally characterized by a velocity gradient α. Then Markstein proposed that the increment in flame-speed ΔS generated by the stretch associated with α can be written in the form

$$\frac{\Delta S}{S_o} = \gamma_m \frac{\alpha\delta}{S_o}, \qquad \text{i.e. } \Delta S = \gamma_m \alpha\delta, \qquad \delta = \frac{\lambda}{M_o C_p}, \quad (9)$$

where $S_o = M_o/\rho_\infty$ is the unperturbed (adiabatic) flame-speed, γ_m is a constant (Markstein number) controlled by the intrinsic properties of the mixture, such as the Lewis number, and δ is a measure of the thickness of the unperturbed flame. However, treating a structure of thickness δ as a discontinuity introduces uncertainty in the flame position of order $O(\delta)$, and a corresponding uncertainty in the value of the gas velocity on the cold side of the flame of order $O(\alpha\delta)$, precisely the magnitude of Markstein's correction to the flame-speed! Resolution of this difficulty, and a rational justification of Markstein's strategy can only come from a more precise specification of the flame location, and a suitable and convenient choice is the flame-sheet location. Then, for a weakly stretched flame, the preheat zone is approximately 1D, and meaningful well-defined corrections to the flame-speed can be calculated [12, 13]. This is possible because the loss or gain of Y within the preheat zone which modifies Eq. (8) can be expressed in terms of local well-defined combustion-field ingredients.

Once one moves firmly away from the 1D configuration, however, the significance of flame-speed is, in general, lost. Consider, for example, the counterflow of fresh mixture and inert, the latter supplied at a temperature equal to the adiabatic flame-temperature

$$T_{ad} = T_\infty + \frac{Q}{C_p} Y_\infty. \quad (10)$$

The gas velocity is

$$\mathbf{q} = \alpha(-x, y) \ \ (\rho = \text{constant}). \quad (11)$$

If the Lewis number Le $(= \lambda/\rho\mathscr{D}C_p)$ is equal to 1, T and Y are related via the Schwab–Zeldovich relation

$$T + \frac{Q}{C_p} Y = T_{ad}, \quad (12)$$

whence

$$T_* = T_{ad} \quad (13)$$

and the flame-strength (reactant consumption rate) is fixed, independently of α. The flame-sheet positions itself at a station x_* so that the flux condition (7) is satisfied $(n = x)$, and the only way to construct a speed is via the product αx_* (the gas speed at the flame-sheet) but this has no physical importance, is a measure only of itself.

This is the general situation for unsteady flames, multi-dimensional flames, and flames interacting with boundaries. Physical discussions of these situations which appeal to the concept of flame-speed, appeal to an illusion. A corollary of this is that attempts to construct general theories relating flame-speed in a non-linear fashion to stretch, curvature, or other measures of the environment, are futile.

Consider, for example, the classical discussion of flame-holding at a burner rim [14]. What is sketched in Fig. 2 is the flame-sheet whose distance from the rim is measured on the scale of the preheat zone, and which is assumed to carry, as an intrinsic property, a speed, a speed that varies according to the heat loss to the rim because of a well-defined temperature dependence. Two equilibrium positions are defined (A, B) where B, on the basis of a quasi-steady argument (flame displacement), is stable. But the flame-speed in this discussion, if it exists, must originate in Eq. (7),

yet the connection has not been made. That the *conclusion* is correct, that stability is predicted, is unconvincing, for the argument has but two outcomes and it takes little ingenuity in situations such as this to ensure the correct one.

Our conclusion then is that flame-speed is only a relevant concept in a narrow context, that of the unbounded flat flame, close approximations thereto, or certain special cases.[1,2] Elsewhere, it is 21st century phlogiston.

The edge-speeds that we shall discuss in later sections are also only meaningful in a narrow context, and an 'explanation' of edge-flame holding is as elusive as the holding of Fig. 2.

3. One-dimensional diffusion flames

Consider the counterflow of fuel and oxidizer, modeled by the equations

$$-\rho\alpha x\frac{\partial}{\partial x}(X,Y,C_pT) = \frac{\partial^2}{\partial x^2}(\rho\mathscr{D}_X X,\rho\mathscr{D}_Y Y,\lambda T) + (-\alpha_X,-\alpha_Y,Q)BXY\,e^{-E/RT}, \tag{14}$$

$$x\to-\infty: X\to X_\infty,\ Y\to 0,\ T\to T_\infty;$$

$$x\to+\infty: X\to 0,\ Y\to Y_\infty,\ T\to T_\infty.$$

Solutions to this system are characterized by an S-shaped response of maximum temperature to Damköhler number ($\sim B/\alpha$), Fig. 3, a result of significance in edge-flame studies.

In the limit $D\to\infty$ (the Burke–Schumann limit), both X and Y vanish at a thin flame-sheet. Moreover, for typical values of the activation energy, the sheet remains thin and these conditions remain satisfied along the entire upper branch of Fig. 3. Thus, at the sheet,

$$X=0, \tag{15a}$$

$$Y=0, \tag{15b}$$

$$\frac{\rho\mathscr{D}_Y}{\alpha_Y}\left[\frac{\partial Y}{\partial x}\right]-\frac{\rho\mathscr{D}_X}{\alpha_X}\left[\frac{\partial X}{\partial x}\right]=0, \tag{15c}$$

[1] Thus for a steady 1D flame attached to a burner at whose face flux conditions are applied, viz. $MY-\rho\mathscr{D}\,\partial Y/\partial n=MY_\infty$, we have $MY_\infty=-\rho\mathscr{D}(\partial Y/\partial n)_-$, as for the unbounded flame.

[2] Thus Faeth and co-workers, in a series of papers (Ref. [15] and references therein) have measured flame-speeds for outwardly propagating spherical flames of various types by examining flame-sheet trajectories (identified using shadowgraph techniques) and have successfully fitted the results to the *non-linear* flame-speed/flame-stretch equation $S_o/S=1-\gamma_m K_a$ where K_a is the Karlovitz number (the non-dimensional stretch) and γ_m is a constant Markstein number. This formula can be approximated by the classical linear speed/stretch relation (e.g. Eq. (9) when K_a is small.

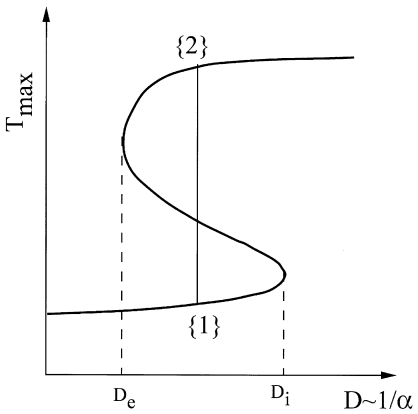

Fig. 3. Variations of maximum temperature with Damköhler number for a diffusion flame in a straining flow.

$$\frac{\rho\mathscr{D}_X}{\alpha_X}\left[\frac{\partial X}{\partial x}\right]+\frac{\lambda}{Q}\left[\frac{\partial T}{\partial x}\right]=0, \tag{15d}$$

(the square brackets signify jumps) where Eq. (15c) is a statement that the reactant fluxes to the sheet must be in stoichiometric proportion, and Eq. (15d) is a statement of energy conservation. In most configurations, Eqs. (15a)–(15c) fix the flame position, and Eq. (15d) determines the flame-temperature $T_*=T_{bs}$, the Burke–Schumann flame-temperature. The flame-sheet structure controls the $O(\varepsilon)$ short-fall of T_* from T_{bs} when D is reduced to finite values, with extinction occurring (at $D=D_e$) when this short-fall is too large [16]. Although a flame-speed could be defined (by the gas-speed normal to the flame-sheet) it is not a significant measure of anything, is no more meaningful than the flame-speed of a deflagration in a strong counterflow.

4. Edge-flames

We shall now see how an edge-flame, a 2D structure, can be constructed from the 1D response of Fig. 3. For a finite interval (D_e, D_i) there are three equilibrium 1D solutions, of which $\{1\}$, on the weak-burning branch, and $\{2\}$, on the strong-burning branch, are stable. These solutions $(X_{\{1\}},X_{\{2\}},Y_{\{1\}},\ldots)$ can be used as boundary-conditions for 2D unsteady generalizations of Eq. (14), viz.

$$\left(\rho\frac{\partial}{\partial t}-\rho\alpha x\frac{\partial}{\partial x}\right)(X,Y,C_pT) = \left(\frac{\partial^2}{\partial x^2}+\frac{\partial^2}{\partial z^2}\right)(\rho\mathscr{D}_X X,\rho\mathscr{D}_Y Y,\lambda T) + (-\alpha_X,-\alpha_Y,Q)BXY\,e^{-E/RT}, \tag{16}$$

$$x\to-\infty: X\to X_\infty,\ Y\to 0,\ T\to T_\infty;$$

$$x\to+\infty: X\to 0,\ Y\to Y_\infty,\ T\to T_\infty.$$

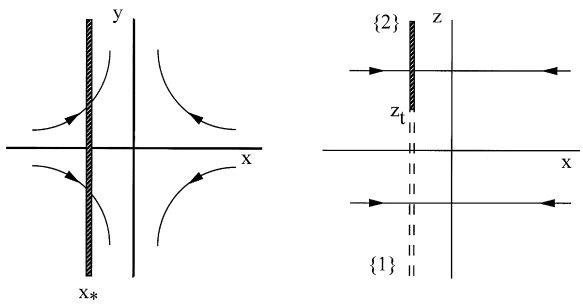

Fig. 4. Schematic of an edge-flame in which the flame-sheet in a counterflow occupies the region $x = x_*$, $z > z_t$.

Specifically, we require (Fig. 4),

$$(X, Y, T) \to (X_{\{1\}}, Y_{\{1\}}, T_{\{1\}}) \text{ as } z \to -\infty,$$
$$(X, Y, T) \to (X_{\{2\}}, Y_{\{2\}}, T_{\{2\}}) \text{ as } z \to +\infty. \tag{17}$$

It is typically the case that the solution $\{1\}$ is weak, essentially quenched, and so, because of the strong temperature dependence of the Arrhenius factor, the 2D flame so described has an edge (at $z \sim z_t$, say) and for $z < z_t$ reaction is negligible, whereas for $z > z_t$ it is vigorous.

Numerical solution of the system (16) and (17) lead to structures which, after initial transients, propagate at well-defined speeds and have unchanging shape. It is this property which gives edge-flames their fundamental status, as fundamental as the classical 1D structures.

The speeds may be positive, corresponding to an *ignition front* advancing into the non-reacting gas (cf. Fig. 1a), or negative, corresponding to a *failure wave*, a retreat of the edge (cf. Fig. 1e), and the edge structures are different in the two cases, Fig. 5. An ignition front is characterized by significant premixing which, together with the trailing diffusion flame, defines a three-branched structure, a *tribrachial flame*, Fig. 5a. The reaction rate displays a strong maximum. On the other hand, a failure wave is essentially a 2D diffusion flame,

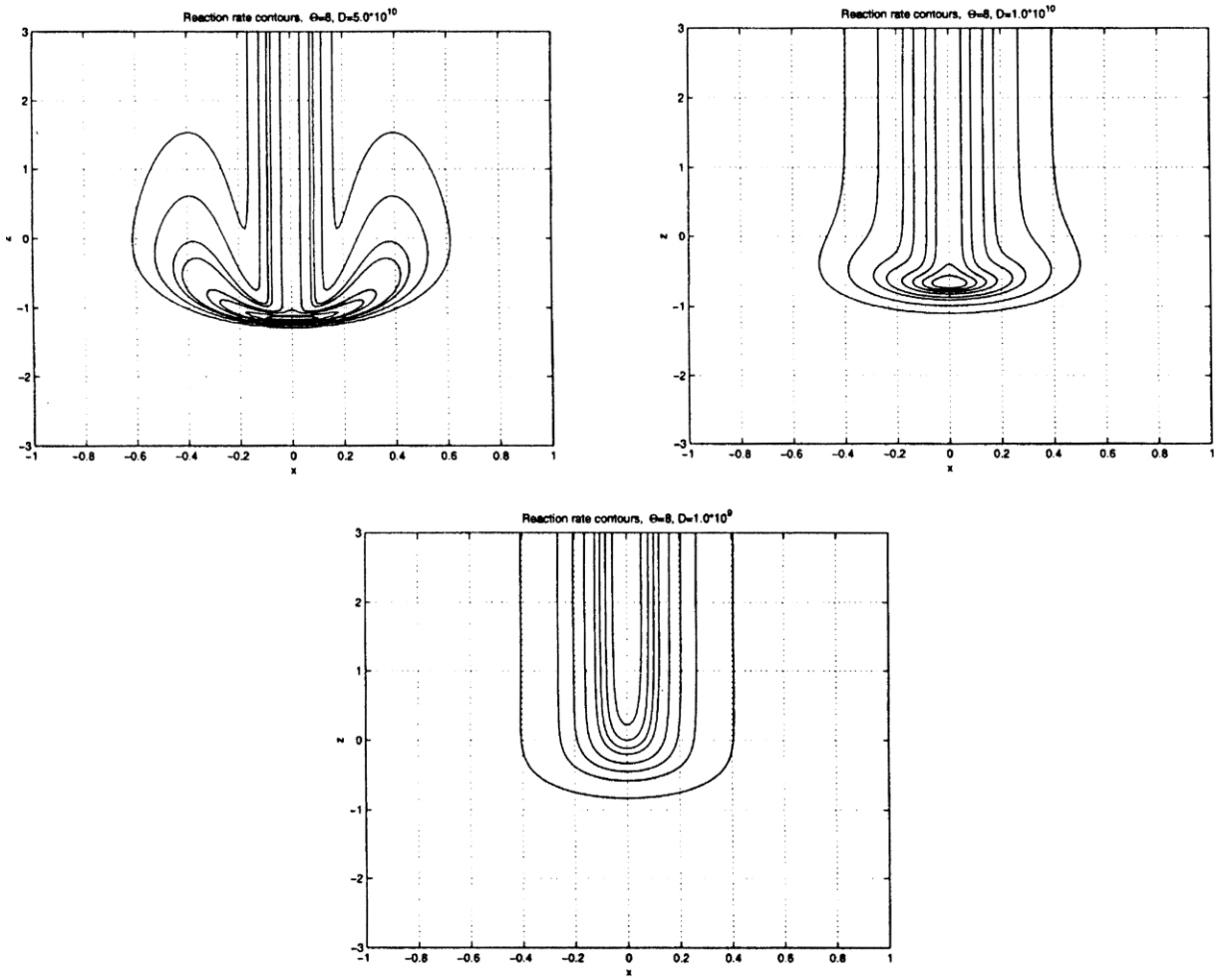

Fig. 5. Reaction-rate contours for advancing (top left panel), stationary (top right panel), and retreating (bottom panel) edge-flames, from Ref. [60], with permission.

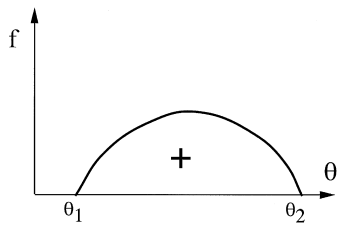

Fig. 6. The source term for a deflagration, cf. Eq. (20).

with no rate maximum in the neighborhood of the edge, Fig. 5c.

Figures similar to those of Fig. 5 were first reported in Ref. [17]. Other calculations have been carried out using detailed chemical models and a full accounting of the Navier–Stokes equations [18,19].

4.1. Understanding edge-speeds

A striking difference between edge-flames and deflagrations is that whereas the latter only have positive propagation speeds, the former can have propagation speeds of either sign. Insight into these properties can be obtained by an examination of the equation

$$\frac{\partial\theta}{\partial t} = \frac{\partial^2\theta}{\partial z^2} + f(\theta, D), \tag{18}$$

where f is a reaction term that depends on a parameter D. We seek solutions corresponding to a traveling wave, i.e.

$$\theta = \theta(z + Vt) \tag{19}$$

whence

$$V\frac{\mathrm{d}\theta}{\mathrm{d}z} = \frac{\mathrm{d}^2\theta}{\mathrm{d}z^2} + f(\theta, D), \tag{20}$$

to be solved subject to the boundary conditions

$$\theta \to \theta_1 \ \text{ as } z \to -\infty, \qquad \theta \to \theta_2 \ \text{ as } z \to +\infty. \tag{21}$$

Interesting and important questions of existence and uniqueness arise in the discussion of the system (20) and

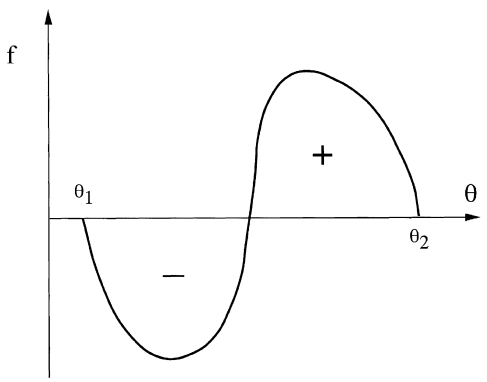

Fig. 7. The source term for a system displaying bistable equilibrium, cf. Eq. (20).

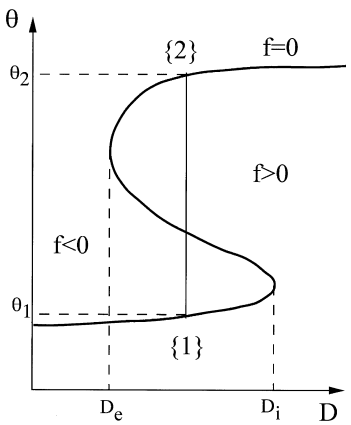

Fig. 8. The level surface $f(\theta, D) = 0$ for a system displaying bistable equilibrium. Along the path from {1} to {2}, D fixed, f varies as in Fig. 7.

(21), but these do not concern us here, and we shall assume that f has the properties necessary for our statements to be meaningful. Clearly f must vanish at $\theta = \theta_1$ and $\theta = \theta_2$.

If Eq. (20) is multiplied by $\mathrm{d}\theta/\mathrm{d}z$ and integrated over the entire real line, we derive the formula

$$V\int_{-\infty}^{+\infty}\left(\frac{\mathrm{d}\theta}{\mathrm{d}z}\right)^2 \mathrm{d}z = \int_{\theta_1}^{\theta_2} f(\theta, D)\mathrm{d}\theta, \tag{22}$$

and this can tell us something about the sign of V. There are two cases that are of interest to us:

Case I: $f \geq 0$ (Fig. 6). Then the r.h.s. of Eq. (22) is positive, so that $V > 0$. This is relevant to deflagrations and indeed, when the Lewis number equals 1, the system (1) yields the structure equation

$$\rho C_\mathrm{p} V\frac{\mathrm{d}T}{\mathrm{d}z} = \lambda\frac{\mathrm{d}^2T}{\mathrm{d}z^2} + BC_\mathrm{p}(T_\mathrm{ad} - T)\mathrm{e}^{-E/RT}H(T - T_\mathrm{c}), \tag{23}$$

which has the form (20). (Here the cut-off function H is introduced to take care of the cold-boundary difficulty).

Case II: *f has the form sketched in* Fig. 7. Typically we are interested in examples where the level surface $f = 0$ defines an S-shaped curve in the θ–D plane, Fig. 8, so that the graph Fig. 7 is correct in the interval $D_\mathrm{e} < D < D_\mathrm{i}$. The variations in Fig. 7 are then the variations along the line {1}–{2} in Fig. 8, one that joins the lower branch to the upper branch. Clearly, if D is close to D_e the negative contribution of f to the integral in Eq. (22) dominates, and V is negative. On the other hand, if D is close to D_i, the positive contribution dominates, and V is positive. There is a unique value of D for which $V = 0$.

Although there are no 1D examples in combustion of this nature, the system (20) and (21) for this case is a 1D analog of edge-flames. Clear links can be forged with some elementary modeling.

5. A one-dimensional model of an edge-flame

The temperature equation

$$V\frac{\mathrm{d}\theta}{\mathrm{d}s} - \frac{\mathrm{d}^2\theta}{\mathrm{d}s^2} = (\theta_\mathrm{w} - \theta) + D(1-\theta)^2 \exp\frac{1}{\varepsilon}\left(1 - \frac{1}{\theta}\right) \quad (24)$$

is an example of Eq. (20) in which f (the r.h.s.) has the properties of Figs. 7 and 8. The second term in f is a true kinetics term with an Arrhenius factor $\mathrm{e}^{-1/\varepsilon\theta}$, and a factor $(1-\theta)^2$ originating in a reactant concentration dependence. The first term, $(\theta_\mathrm{w} - \theta)$, accounts for transport to the side (the x-direction in Fig. 4), transport which carries heat from the flame to the reactant supply boundaries, and carries reactants from those boundaries to the flame. One-dimensional equations of this type have been used in the discussion of fire-spread problems [20], but without the factor $(1-\theta)^2$ or anything similar, a factor which simulates diffusion-limiting in the limit $D \to \infty$. In this section we shall say something about a modeling strategy that leads to Eq. (24). Complete details can be found in Ref. [21].

We start with equations that describe an unsteady combustion field in the x–z plane (cf. Eq. (16))

$$\rho\frac{\partial}{\partial t}(C_\mathrm{p}T, X, Y) - \frac{\partial^2}{\partial z^2}(\lambda T, \rho\mathscr{D}_X X, \rho\mathscr{D}_Y Y)$$
$$= (S_T, S_X, S_Y) + (Q\Omega_T, -\Omega_X, -\Omega_Y). \quad (25)$$

Here S_T, S_X and S_Y are 'side-terms', terms that represent convective or diffusive transport in the x-direction (Fig. 4) and Ω_T, Ω_X and Ω_Y are reaction terms that we shall discuss later.

Underlying Eq. (25) is a 1D system obtained by setting the t- and z-derivatives equal to zero, with solutions that are characterized by an S-shaped response such as that of Fig. 3. Eqs. (25) then describe an evolution in z, unsteady, between 1D solutions characterized by the points {1} and {2}. The details of these solutions (maximum temperature, etc.) are fixed by the choice of the Damköhler number.

In order to reduce Eq. (25) to 1D form, it is necessary to model the side terms in some fashion. Since the combustion field loses heat to the boundaries, we replace S_T :

$$S_T \to -\frac{\lambda(T_\mathrm{w} - T)}{L^2} \quad (26)$$

where L is a length scale characterizing variations in the x-direction (e.g. $L = \sqrt{\lambda/\rho\alpha C_\mathrm{p}}$ for the counterflow problem, Eq. (16)), and T_w is a characteristic or heat-sink temperature. Similar replacements are made for S_X and S_Y so that now Eqs. (25) describes the evolution of averaged quantities, although the precise nature of this average is not defined. This type of bulk modeling is common in engineering applications.

It is also necessary to model the reaction terms, providing some representation of the average over the x-direction. A simple choice—perhaps the simplest—that preserves the functional form of the point-wise description as much as possible, is

$$\Omega_T = \mathfrak{D}(X - X_\mathrm{a})(Y - Y_\mathrm{a})\mathrm{e}^{-E/RT} \quad (27)$$

with similar representations for Ω_X and Ω_Y, where X_a and Y_a are constants. One-dimensional equilibrium is defined by setting the r.h.s. of Eqs. (25) equal to zero, and the fast-chemistry approximation to this equilibrium ($\mathfrak{D} \to \infty$) is characterized by $X = X_\mathrm{a}$, $Y = Y_\mathrm{a}$, an averaged representation of the Burke–Schumann limit.

Certain subtleties need to be addressed in this procedure, which we will not describe here, but Eq. (24) emerges in a plausible fashion when $Le_X = Le_Y = 1$ and Schvab–Zeldovich relations can be invoked. It is non-dimensional, and its variables are connected to those of Eqs. (25) by the formulas:

$$\frac{\partial}{\partial t} = U\frac{\partial}{\partial z}, \qquad s = \frac{z}{L}, \qquad V = \frac{\rho C_\mathrm{p} L U}{\lambda},$$
$$\theta \propto T, \qquad \varepsilon \propto \frac{1}{E}, \qquad D \propto L^2\mathfrak{D}. \quad (28)$$

5.1. Equilibrium

Equilibrium is defined by

$$\theta - \theta_\mathrm{w} = D(1-\theta)^2 \exp\frac{1}{\varepsilon}\left(1 - \frac{1}{\theta}\right) = \Omega \quad (29)$$

and this defines an S-shaped response in the θ–D plane. On the top branch, when ε is small, θ is close to 1 and we write

$$\theta = 1 + \varepsilon\phi, \qquad \varepsilon \to 0,$$
$$\hat{D} = \varepsilon^2 D(1-\theta_\mathrm{w})^{-1} = \mathrm{O}(1), \quad (30)$$

whence

$$\phi^2\,\mathrm{e}^{\phi} = \hat{D}^{-1}, \quad (31a)$$

$$\Omega = 1 - \theta_\mathrm{w} = \mathrm{O}(1). \quad (31b)$$

Extinction occurs when $\phi = -2$, $\hat{D} = \frac{1}{4}\mathrm{e}^2$, and there is no strong-burning solution if $\hat{D} < \frac{1}{4}\mathrm{e}^2$. If one proceeds down the S-shaped response, ϕ vanishes at $\hat{D} = \infty$, decreases as the top branch is traversed, reaches the value (-2) at the turning point, and continues to decrease down the middle branch.

An important role is played by $\mathrm{O}(1/\varepsilon)$ values of $\hat{D}$, viz.

$$\hat{D} = \varepsilon^{-1}D_1, \qquad D_1 = \mathrm{O}(1), \quad (32)$$

whence, on the top branch,

$$\theta = 1 - \frac{\varepsilon\sqrt{\varepsilon}}{\sqrt{D_1}} + \cdots \quad (33)$$

D_1 is a Damköhler number that controls the equilibrium state. In particular it controls the post-edge temperature via Eq. (33) and therefore the 'reactant leakage'.

5.2. Steady asymptotic solution of an unbounded edge-flame, $D = O(1/\varepsilon 3)$

The asymptotic structure in the limit $\varepsilon \to 0$, $D_1 = O(1)$ ($D = O(1/\varepsilon^3)$), is similar in many respects to that of a deflagration. If the edge is located at $s = 0$, then in $s < 0$ reaction is frozen, because of the low temperature, and across the edge, or thin reaction zone, there is a jump in the first derivative of θ. Behind the edge, $\theta = 1$ to first order, cf. Eq. (33). The cold equilibrium at $s = -\infty$, defined by a point on the lower branch of the S-shaped response, is $\theta = \theta_w$ with error that is exponentially small in ε; it is commonly the case in edge-flame configurations that reaction is negligible on the cold side of the edge, that solution {1} is essentially the frozen solution.

In the preheat zone ($s < 0$),

$$\theta = \theta_w + (1 - \theta_w)e^{\nu s}, \qquad \nu = \tfrac{1}{2}[V + \sqrt{V^2 + 4}]. \tag{34}$$

Within the reaction zone, of thickness ε,

$$\theta = 1 + \varepsilon\phi_2(\xi) + \cdots, \qquad s = \varepsilon\xi \tag{35}$$

where

$$\phi_2 \to 0 \ \text{ as } \xi \to \infty \tag{36}$$

to match with the equilibrium solution (33). In the usual way (see the earlier discussion of the deflagration structure) the gradient as $\xi \to -\infty$ can be determined and matched with the gradient defined by Eq. (34). Indeed,

$$\frac{d\theta}{ds_-} = 2\sqrt{\varepsilon^3 D}, \tag{37}$$

whence

$$V + \sqrt{V^2 + 4} = 2\Psi \equiv \frac{4\sqrt{D_1}}{\sqrt{1 - \theta_w}}, \tag{38}$$

i.e.

$$V = \Psi - \frac{1}{\Psi} \tag{39}$$

which defines a positive or negative speed accordingly as $\Psi > 1$ or $\Psi < 1$.

In the infinite Damköhler number limit $\Psi \to \infty$,

$$V \to \Psi \tag{40}$$

and it is natural to identify this with the adiabatic flame-speed for a deflagration in a stoichiometric mixture. (That an edge-flame cannot exist in the limit since it puts D beyond the ignition value D_i is of no concern, since the ignition value is exponentially large in ε). For the counterflow problem, when account is taken of the dependence of V and Ψ on the reference length $L \propto 1/\sqrt{\alpha}$, Eq. (39) is equivalent to $U/S_o = 1 - \alpha/\alpha_0$, where α_0 is defined by $\Psi = 1$.

The variations in the reaction rate within the edge-flame structure are consistent with numerical solutions of the 2D problem for non-negative edge-speeds. Ahead of the edge, reaction is frozen (exponentially small), within an $O(\varepsilon)$ neighborhood of the edge it is $O(1/\varepsilon)$ ($\sim d^2\theta/ds^2$), and in the post-edge equilibrium region it is O(1). This structure is sketched in Fig. 9.

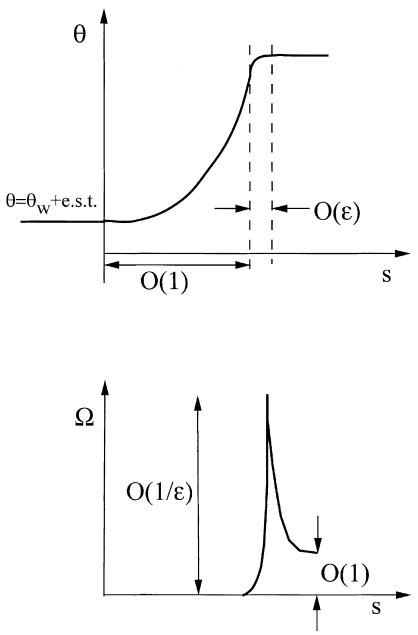

Fig. 9. Temperature variations and reaction-rate variations through the flame-edge, 1D model, $D = O(1/\varepsilon^3)$. (e.s.t.: exponentially small terms).

Finally, before leaving this section, it is useful to note the important distinctions between the present solution and that of the classical deflagration. There is no cold-boundary difficulty, since the state at $s \to -\infty$ is defined by an equilibrium point fixed by the Damköhler number. Similarly, the flame-temperature, a characteristic of the post-edge equilibrium state, is defined by the Damköhler number. Mixing occurs ahead of the edge, but to say there is a mixture at $s \to -\infty$ is quite different from saying that there is an equilibrium point characterized by substantial reactant leakage through the reaction zone. The former will support a deflagration (an ignition wave) if ignited, whereas the latter may or may not, depending on the Damköhler number. Here the side terms play a crucial role. For a deflagration (no side terms) the preheat zone thickness ranges from 0 to ∞ as the propagation speed varies from ∞ to 0, but for the edge-flame the corresponding thickness (ν^{-1}) spans the same range for speeds varying from ∞ to $-\infty$. Decrease the Damköhler number (and so increase the thickness) in a deflagration and the speed will decrease, but always be positive. Decrease the Damköhler number in an edge-flame and the speed will become negative. For an edge-flame there is a watershed value of the Damköhler number ($\Psi = 1$) for which the edge-speed is zero. At larger Damköhler numbers ($\Psi > 1$) the hot post-edge flame is an ignition source for the cold

mixture ahead of the edge; at smaller Damköhler numbers ($\Psi < 1$) the cold ante-edge mixture quenches the post-edge flame.[3]

5.3. Steady asymptotic solution of an unbounded edge-flame, $D = O(1/\varepsilon 2)$

The discussion of Section 5.2 is concerned with $O(1/\varepsilon)$ values of $\hat{D}$, although edge-flames can exist for O(1) values, and a different asymptotic treatment is necessary in this case.

We seek a solution of Eq. (24) for which $D\varepsilon^2 = O(1)$. It then turns out that $V = O(1/\sqrt{\varepsilon})$, $V < 0$. Since Ψ is $O(\sqrt{\varepsilon})$, it follows that $U/S_o = V/\Psi = O(1/\varepsilon)$. If, as before, the edge is located at $s = 0$, reaction is negligible in $s < 0$ and, because $|V|$ is large, diffusion can also be neglected. We write

$$s = -V\sigma = O(1/\sqrt{\varepsilon}) \tag{41}$$

whence

$$\frac{d\theta}{d\sigma} - (\theta - \theta_w) = 0, \quad \sigma < 0 \tag{42}$$

to first order, with solution

$$\theta = \theta_w + (1 - \theta_w)e^{\sigma}. \tag{43}$$

The edge itself is described in terms of the variables

$$\sigma = \varepsilon\xi, \qquad \theta = 1 + \varepsilon\phi(\xi), \qquad (s = O(\sqrt{\varepsilon})) \tag{44}$$

whence

$$-\frac{d\phi}{d\xi} - \frac{1}{\varepsilon V^2}\frac{d^2\phi}{d\xi^2} = (1 - \theta_w)[\hat{D}\phi^2 e^{\phi} - 1]. \tag{45}$$

The boundary conditions are

$$\xi \to \infty : \phi \to \phi_1 \text{ where } \hat{D}\phi_1^2 e^{\phi_1} = 1 \tag{46}$$

cf. Eq. (31a),

$$\xi \to -\infty : \frac{d\phi}{d\xi} \to (1 - \theta_w) \tag{47}$$

to match with the gradient of Eq. (43).

If we write

$$\frac{d\phi}{d\xi} = (1 - \theta_w)P(\phi) \tag{48}$$

the problem reduces to a first order boundary-value problem

$$-\frac{(1 - \theta_w)}{\varepsilon V^2}P\frac{dP}{d\phi} = P + \frac{\phi^2}{\phi_1^2}e^{\phi - \phi_1} - 1, \tag{49}$$

$$P(\phi_1) = 0, \qquad P(-\infty) = 1$$

[3] This ignition/quenching dichotomy occurs in classical ignition studies in which a ball of hot burnt gas is placed in an atmosphere of cold fresh mixture: whether the ball ignites the mixture or the mixture quenches the reaction initiated at the ball boundary, depends on the size of the ball. For this problem the effective Damköhler number is proportional to the square of the ball diameter.

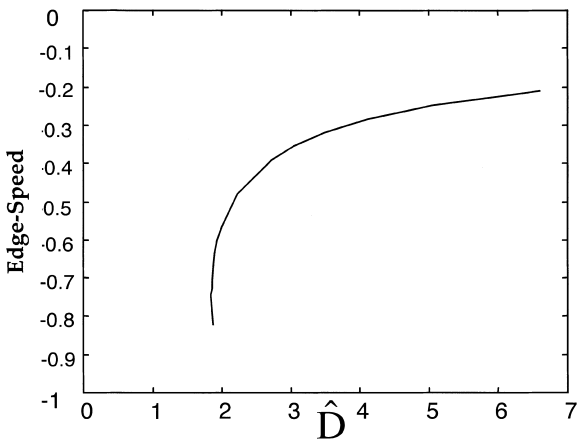

Fig. 10. Variations in the speed of a failure wave with Damköhler number, 1D model, $D = O(1/\varepsilon^2)$.

from which the eigenvalue $\varepsilon V^2/(1 - \theta_w)$ can be determined; we are concerned with the range $-2 < \phi_1 < 0$, corresponding to the upper branch of the equilibrium solution.

Numerical solution of Eq. (49) determines the eigenvalue as a function of ϕ_1, and therefore $\hat{D}$, variations of which are shown in Fig. 10. These solutions are not accurate for realistic values of ε (e.g. $\varepsilon = 1/16$), but capture the fundamental behavior and physics. These rapidly retreating failure waves are much thicker than the ignition fronts, and the reaction rate within the edge and behind it is O(1), cf. Fig. 5c. The structure is sketched in Fig. 11.

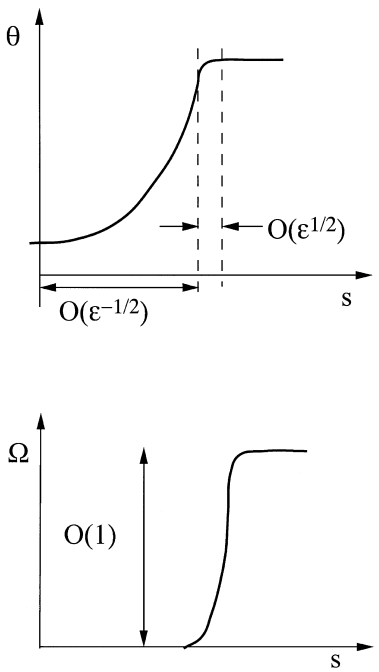

Fig. 11. Temperature variations and reaction-rate variations through the edge-flame, 1D model, $D = O(1/\varepsilon^2)$.

Our discussion here is valid when both Lewis numbers are equal to 1. Although attempts have been made to relax this restriction, a satisfactorily robust model has yet to be developed [21,22].

6. Two-dimensional descriptions of edge-flames

The 1D model of edge-flames is of conceptual value, linking the subject to the classical reaction-diffusion equation (18) for functions f exhibiting bistable equilibrium, e.g. [23], and it captures some of the essential physics, but it is a predictive tool of uncertain reliability and cannot substitute for a 2D treatment. The asymptotics in this case was pioneered by Dold, and we shall sketch some of the results that he and his colleagues have obtained.

It is a characteristic of edge-flames of the kind we have discussed so far that significant mixing of reactants occurs on the low temperature side of the edge. Thus, with reaction neglected, Eqs. (14) have solutions (when $\mathscr{D}_X = \mathscr{D}_Y = \mathscr{D}$)

$$X = \frac{1}{2}X_\infty\left[1 - \operatorname{erf}\left(x\sqrt{\frac{\alpha}{2\mathscr{D}}}\right)\right],$$
$$Y = \frac{1}{2}Y_\infty\left[1 + \operatorname{erf}\left(x\sqrt{\frac{\alpha}{2\mathscr{D}}}\right)\right] \tag{50}$$

and the corresponding mixture varies (with x) from fuel lean to fuel rich. Edge-flames are thus connected to the problem of propagation in a stratified mixture, an early experimental report of which can be found in Ref. [24]. The first analysis, for weak stratification, is due to Dold [25], although we shall follow here the argument presented in Ref. [26].

Imagine a deflagration sustained by a mixture moving in the z-direction in which the fuel and oxidizer concentrations vary linearly with x, Fig. 12. Suppose the mixture is in stoichiometric proportion on the z-axis, fuel-lean in $x < 0$, and fuel-rich in $x > 0$. Then the burnt gas will contain hot unburnt oxidizer in $x < 0$, hot unburnt fuel in $x > 0$, and these excess reactants will diffuse towards each other to generate a diffusion flame that trails the two branches of the premixed flame. We shall call this a tribrachial flame (Fig. 5a), a name first used in 1988 [27], with firm roots in the English language. We use the kinetics of Eqs. (14), a two-component model, with $\alpha_X = \alpha_Y = 1$, and both Lewis numbers equal to 1.

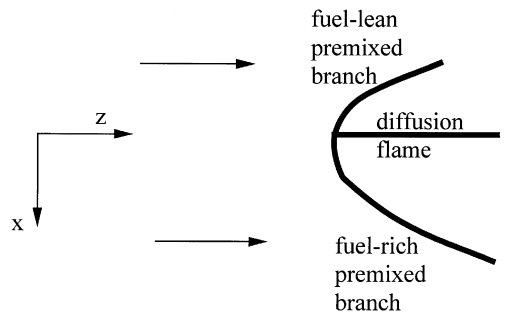

Fig. 12. The tribrachial flame supported by weak mixture gradients in the supply, cf. Fig. 5a.

Consider a plane deflagration with supply conditions

$$T \to T_\mathrm{f},\quad X \to X_\mathrm{f} = X_0 + \varepsilon X_1,$$
$$Y \to Y_\mathrm{f} = Y_0 + \varepsilon Y_1 \ \text{ as } z \to -\infty \tag{51}$$

where

$$X_0 = Y_0 \tag{52}$$

and

$$\frac{1}{\varepsilon} = \frac{E}{RT_{\mathrm{ad}0}} \gg 1, \tag{53}$$

where

$$T_{\mathrm{ad}_0} = T_\mathrm{f} + \frac{QX_0}{C_\mathrm{p}} = T_\mathrm{f} + \frac{QY_0}{C_\mathrm{p}} \tag{54}$$

is the adiabatic flame-temperature at stoichiometry when $X_1 = Y_1 = 0$. Then the standard procedure (cf. our earlier discussion of the deflagration for a one-component model) leads to the following expression for the mass flux:

$$M = M_0 \exp\left[\frac{X_1 Q}{2C_\mathrm{p}T_{\mathrm{ad}_0}}\right]\left[1 + \frac{(Y_1 - X_1)Q}{2C_\mathrm{p}T_{\mathrm{ad}_0}}\right]^{1/2},$$
$$Y_1 \geq X_1,$$
$$M = M_0 \exp\left[\frac{Y_1 Q}{2C_\mathrm{p}T_{\mathrm{ad}_0}}\right]\left[1 + \frac{(X_1 - Y_1)Q}{2C_\mathrm{p}T_{\mathrm{ad}_0}}\right]^{1/2}, \tag{55}$$
$$X_1 \geq Y_1.$$

Here, M_0 is the value of M when $X_1 = Y_1 = 0$.

Now suppose that

$$X_1 = -\beta\frac{x}{\delta}, \qquad Y_1 = \beta\frac{x}{\delta} \tag{56}$$

where

$$\delta = \frac{\lambda}{M_0 C_\mathrm{p}}, \tag{57}$$

the nominal thickness of the undisturbed flame, and β is an assigned parameter. Then, when β is small, Eqs. (55) yield

$$M = M_0\left[1 - \frac{Q^2\beta^2x^2}{4\delta^2C_\mathrm{p}^2T_{\mathrm{ad}_0}^2}\right] \tag{58}$$

corresponding to a weakly curved flame, with shape

$$z = \frac{Q\beta x^2}{2\sqrt{2}\delta C_\mathrm{p}T_{\mathrm{ad}_0}}. \tag{59}$$

If kinematics were the whole story these results would complete it. We have assumed that the flame is stationary in a flow of mass flux M_0, and the only necessary accommodation to the mixture gradient is that the flame curve so that the normal mass flux is M, as defined by Eq. (58). However,

as a consequence of the curvature, the flame experiences stretch—a pseudo-Lagrangian area increase here generated by a non-vanishing velocity component parallel to the sheet—and a stretched flame does not travel at the adiabatic flame-speed. The stretch, equal to $M_0 Q\beta/\sqrt{2}\delta C_p \rho T_{ad_0}$, is small, and there is a universal relation between small stretch and the flame-speed perturbation that it generates (the Markstein correction, discussed earlier). This correction may be calculated for a flame in a uniform mixture ($X_1 = Y_1 = 0$) since the two small effects (of concentration gradient and stretch) are, to first order, additive. (We identify the flame position with the flame-sheet position.) In this way we conclude that the flame travels at a speed corresponding to a mass flux

$$M_0\left[1 - \frac{Q\beta\sqrt{2}}{C_p T_{ad_0}}\right]. \tag{60}$$

The flame is slowed by the gradient. Note that M_0, the mass flux associated with supply values $X = X_0 = Y_0 = Y$ is, in the 2D context, defined by the values of X and Y at the stoichiometric level surface defined by the mixing solution (50), so that $X_0 = Y_0 = \frac{1}{2}X_\infty = \frac{1}{2}Y_\infty$.

A treatment of weakly stretched tribrachial flames when Le_Y is different from 1 is described in Ref. [28]. The results are as one would expect from the effect of Lewis number on weakly stretched deflagrations, and are briefly described later.

When $\beta \sim X_0$, X changes by $O(\varepsilon X_0)$ and Y changes by $O(\varepsilon Y_0)$ amounts for $O(\delta)$ changes in x, and the flame-speed of each deflagration branch changes by $O(S_o)$ amounts in this distance, so that the radius of curvature of the edge-flame is comparable to δ. In this case an asymptotic treatment is possible, but it leads to a non-linear integral equation that can only be solved numerically [29]. In the context of the gradient generated by a counterflow, a comparison of Eqs. (50) and (51), (56) shows that $\beta \sim X_0$ is equivalent to $\alpha \sim \varepsilon^2\mathscr{D}/\delta^2$. U/S_o (the normalized edge-speed) falls monotonically with α on this scale, approaching 0 as $\alpha\delta^2/\varepsilon^2\mathscr{D} \to \infty$. The distinct flame branches merge in this limit.

Let us now estimate the value of α sufficient to extinguish the 1D diffusion flame. As we have noted, δ is the thickness of the stoichiometric deflagration. The corresponding flame-sheet structure is characterized, in the usual way, by a diffusion-reaction balance in which $X \sim \varepsilon X_\infty$, $Y \sim \varepsilon Y_\infty$, in a region of thickness $\sim \varepsilon\delta$, so that the reactant gradients $\sim X_\infty/\delta$. The magnitude of δ is determined by this balance, and

$$\delta^2 \sim \frac{\rho\mathscr{D}\, e^{1/\varepsilon}}{\varepsilon^3 B X_\infty}. \tag{61}$$

Precisely the same balance and the same estimate for the flame-sheet thickness $\varepsilon\delta$ arises in Liñán's analysis of diffusion-flame quenching [16], but then the concentration gradient X_∞/δ is comparable to $X_\infty\sqrt{\alpha/\mathscr{D}}$ to match with the counterflow structure beyond the flame-sheet, so that $\alpha \sim \mathscr{D}/\delta^2$ at extinction. This is the largest value of α that is of interest.

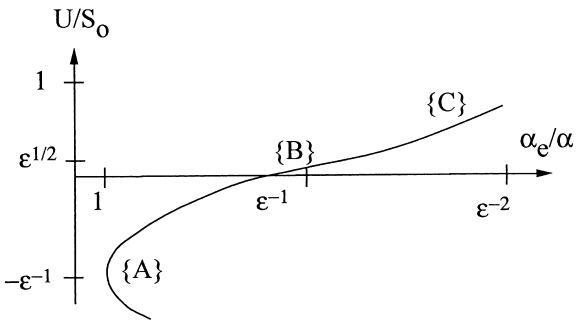

Fig. 13. Schematic showing the variations of edge-speed with inverse rate of strain deduced from 2D asymptotic treatments [30].

Dold [30] has described the asymptotic structure for values of α ranging from $\sim \varepsilon^2\mathscr{D}/\delta^2$ to $\sim \mathscr{D}/\delta^2$, and three distinct analyses are necessary, Fig. 13. Region {C} we have already discussed, corresponding to $U/S_o \sim 1$, $\alpha/\alpha_e \sim \varepsilon^2$ (α_e is the extinction value of α); region {B} corresponds to $U/S_o \sim \sqrt{\varepsilon}$, $\alpha/\alpha_e \sim \varepsilon$; and region {A} corresponds to $U/S_o \sim -1/\varepsilon$, $\alpha/\alpha_e \sim 1$. Region {C} has its counterpart in the 1D model, $D_1 = O(1)$, and if α_0 is the value of α for which the edge-speed is zero we note that $\alpha_0/\alpha_e = O(\varepsilon)$, in agreement with the 1D model. But the latter has only two distinct asymptotic structures (for $\alpha/\alpha_e \sim 1, \varepsilon$), not 3. It is not surprising that details are lost in the brutal simplifications necessary to construct a 1D model.

The type of flame discussed in this section has been usefully analyzed using an approximate strategy in which the flame-sheet is assumed to have the shape of a parabola [31].

7. The edges of deflagrations

Edge-flame theory has strong roots in Phillips's experimental observations of flames in stratified mixtures [24], and because of the way it evolved it was assumed for some years that edge-flames could only exist for non-premixed reactants. Associated with this was a tendency to view edge propagation in the narrow context of the mixing structures at the edge, particularly the tribrachial structure with its twin deflagrations ('the edge propagates because it looks like a deflagration'). But if one views edge-flames in the context of an underlying 1D multiple response, it is clear that they can exist in any combustion context in which there are two stable 1D solutions, and that their wave-like property is rooted in the 1D response.

Multivalued responses occur in a number of configurations containing deflagrations. Consider, for example, the plane counterflow of a fresh mixture and an inert. Provided the inert is at not too high a temperature, variations

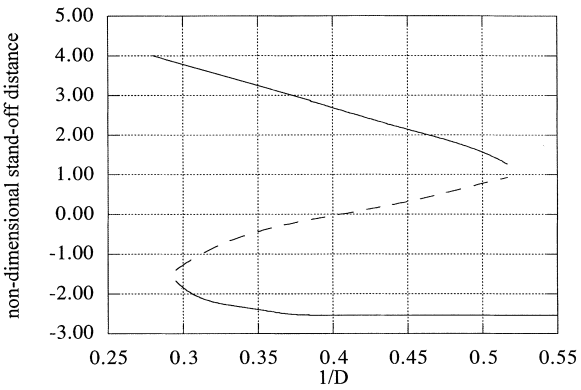

Fig. 14. Position of a premixed flame in a straining flow of fresh mixture and inert, from Ref. [33], with permission. A point on the upper solution branch corresponds to a flame on the fresh-mixture side of the stagnation point, a classical adiabatic deflagration in the limit of vanishing strain.

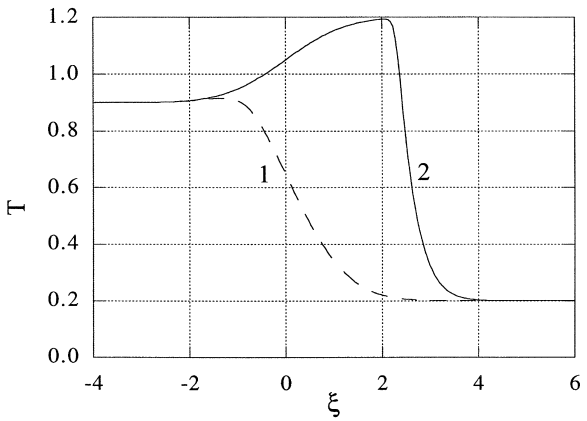

Fig. 15. Temperature profiles for the 'hot' {2} and 'cold' {1} 1D solutions, end solutions for a premixed edge-flame in a fresh/inert counterflow, from Ref. [33], with permission.

of flame-sheet location with the inverse Damköhler number ($\sim\alpha$) are typified by Fig. 14, with a stable upper branch and a stable lower branch. In a finite D-interval, both stable solutions exist simultaneously, and these can be used to define end states for an edge-flame [32,33]. A simple mathematical framework in which this can be done is defined by the equations

$$\left(\rho\frac{\partial}{\partial t}-\rho\alpha x\frac{\partial}{\partial x}\right)(C_pT,Y) = \frac{\lambda}{C_p}\left(\frac{\partial^2}{\partial x^2}+\frac{\partial^2}{\partial z^2}\right)(C_pT,Y)+(Q,-1)BY\,e^{-E/RT}, \quad (62)$$

with boundary conditions

$$x\to-\infty: T\to T_i,\ Y\to 0;$$
$$x\to+\infty: T\to T_f,\ Y\to Y_f; \quad (63)$$

$$z\to-\infty: \text{'cold' solution } T\to T_{\{1\}},\ Y\to Y_{\{1\}},$$
$$z\to+\infty: \text{'hot' solution } T\to T_{\{2\}},\ Y\to Y_{\{2\}}. \quad (64)$$

We have chosen the Lewis number to be 1.

The Schvab–Zeldovich variable

$$\Phi\equiv T+\frac{QY}{C_p} \quad (65)$$

satisfies a reaction-free equation, with steady solution

$$\Phi=T_{ad}+\frac{1}{2}(T_i-T_{ad})\operatorname{erfc}\left(\frac{1}{\sqrt{2}}\xi\right),\quad \xi=x\sqrt{\frac{\rho\alpha C_p}{\lambda}} \quad (66)$$

where $T_{ad}=T_f+QY_f/C_p$ is the adiabatic flame-temperature defined by the fresh supply at $x\to\infty$. Then a single equation, suitably non-dimensionalized, has to be solved, viz.

$$\frac{\partial T}{\partial\tau}-\xi\frac{\partial T}{\partial\xi}=\frac{\partial^2T}{\partial\xi^2}+\frac{\partial^2T}{\partial\zeta^2}+\frac{D}{\epsilon^2}(\Phi-T)\exp\frac{1}{\epsilon}\left(1-\frac{T_{ad}}{T}\right). \quad (67)$$

Sample 1D steady solutions ($\partial/\partial\tau=0=\partial/\partial\zeta$) on the lower and upper branches of Fig. 14 are shown in Fig. 15, and define the boundary conditions (64). Reaction plays little role in the solution {1}.

When Eq. (67) is solved with appropriate initial data (typically, a smooth interpolation between the hot and cold solutions), what emerges depends on the value of D. Near the extinction point ($1/D\approx 0.517$) a failure wave of fixed form emerges once initial transients have decayed; near the ignition point ($1/D\approx 0.294$) an ignition front emerges. Solutions of this kind are shown in Figs. 16 and 17. The hooked nature of the edge can be understood by reference to the limit flame-sheet positions defined by Fig. 14. If the

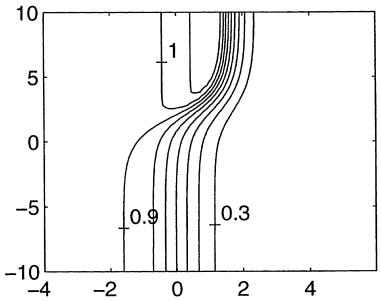

Fig. 16. Temperature contours for a failure wave, a premixed edge-flame in a fresh/inert counterflow, from Ref. [33], with permission. The structure is translating upwards.

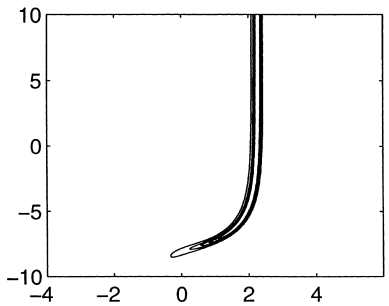

Fig. 17. Reaction-rate contours for an ignition front, a premixed edge-flame in a fresh/inert counterflow, from Ref. [33], with permission. The structure is translating downwards.

dimensional edge-speed is U, a non-dimensional speed is defined by

$$V = \rho U \sqrt{\frac{C_p}{\lambda B}} \frac{1}{\epsilon} e^{1/2\epsilon} \tag{68}$$

variations of which are shown in Fig. 18. Since

$$V = \frac{\rho U}{M_{ad_\infty}} \frac{\sqrt{2T_a}}{T_a - T_f} \tag{69}$$

where M_{ad_∞} is the adiabatic mass flux for the classical deflagration defined in the asymptotic limit $1/\epsilon \to \infty$, comparable to the finite $1/\epsilon$ value, M_{ad}, V is roughly a measure of ρU on the scale M_{ad}.

Note that the flame-sheet pictured in Fig. 17 is translating vertically with unchanging shape, and even when account is made of the x-wise fluid flow (negative for $x > 0$, positive for $x < 0$) the tip of the sheet appears to have a velocity relative to the fluid with components both normal and parallel to the sheet. If one wanted to link the stability dynamics of the configuration of Fig. 2 to a 'flame-speed' it would apparently be necessary to account for advance or retreat of the edge as well as of the sheet itself.

Failure waves of the kind described here have been observed in methane/air flames rising in a standard inflammability tube containing sublimit mixtures [6], Fig. 1e. For such mixtures, the rise speed of the flame and the hot bubble of gas behind it is buoyancy-controlled—following extinction of the flame, the hot gases continue to rise with unchanged speed until they have cooled and buoyancy forces have weakened. Consequently, in a reference frame tied to the rising bubble, the flame is close to a stagnation plane and experiences a straining flow generated by the displacement by the bubble of the cold fluid ahead of the flame. The post-flame gases are cooled by heat losses to the tube walls so that in due course, after the super-combustion initiated by the spark has subsided, the flame is quenched at the centerline by reason of the mechanism identified in Fig. 14. Once the quenching is initiated in this way, it continues via an axisymmetric failure wave that sweeps down the flame from the tip to the skirt. This failure wave propagates because of its innate property, and because of convection by the flow parallel to the flame.

The only other experimental record of edge-flames in mixtures is reported in Ref. [34]. A standard counterflow is used in which high aspect ratio slots deliver the two flows, but are misaligned by a few degrees so that the rate of strain varies across the slot width. In this way an edge-flame can be generated, positioned at that point where the rate of strain is compatible with (essentially) a zero edge-speed. We shall discuss these experiments in a later section.

7.1. The symmetric counter-flow problem

A second combustion field characterized by premixed reactants and a multivalued response is generated by the symmetric counterflow of fresh mixture against fresh mixture. At sufficiently large straining rates the twin flame-sheets interact with each other, and extinction occurs, Fig. 19. In addition, in a context that resolves the cold-boundary difficulty (e.g. a cut-off temperature), there is a

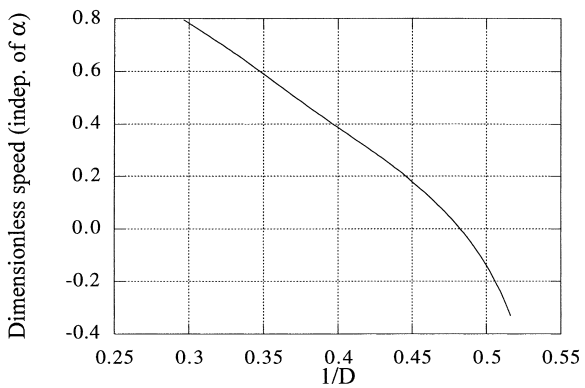

Fig. 18. Variations of edge-speed with inverse Damköhler number ($\sim \alpha$), a premixed edge-flame in a fresh/inert counterflow, from Ref. [33], with permission.

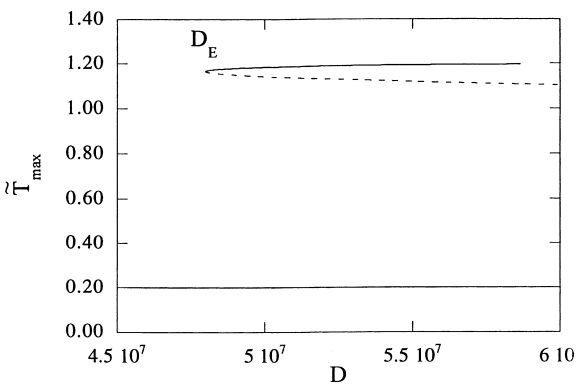

Fig. 19. Flame-temperature vs. Damköhler number, twin deflagrations in a symmetric premixed counterflow, from Ref. [35], with permission.

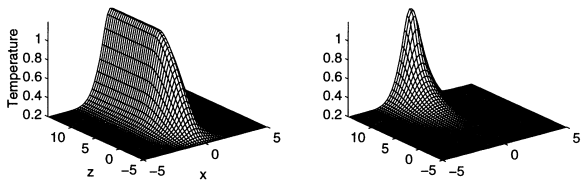

Fig. 20. Temperature topography for a failure wave, twin deflagrations in a symmetric premixed counterflow, from Ref. [35], with permission. The left panel shows the initial structure, the right panel shows the structure when it has retreated almost to the computational boundary.

quenched solution

$$T = T_{\mathrm{f}}, \qquad Y = Y_{\mathrm{f}}, \tag{70}$$

the supply values, here specified at $|x| = \infty$. Apart from the adjustment of the boundary conditions, the mathematical problem is that defined by Eqs. (62)–(65), but now the Schvab–Zeldovich variable Φ has solution

$$\Phi = T_{\mathrm{ad}} \tag{71}$$

and an appropriate non-dimensional equation can be written as

$$\frac{\partial T}{\partial \tau} - \xi\frac{\partial T}{\partial \xi} = \frac{\partial^2 T}{\partial \xi^2} + \frac{\partial^2 T}{\partial \zeta^2} + D(T_{\mathrm{ad}} - T)\exp\left(-\frac{E}{R\,\Delta T}\,\frac{1}{T}\right), \tag{72}$$

$$D = \frac{B}{\rho\alpha}, \qquad \Delta T = T_{\mathrm{ad}} - T_{\mathrm{f}}.$$

Failure wave and ignition front solutions are shown in Figs. 20 and 21 [35]. Insofar as edge-speed variations are concerned it should be noted that an error in the scaling used in Fig. 4 of Ref. [35] suggests that the edge-speed exceeds the adiabatic flame-speed for large D, but in fact $\rho U \leq M_{\mathrm{ad}}$, equality prevailing in the limit.

7.2. Deflagration with radiation losses

The third example of a deflagration with an edge is rooted in the 1D deflagration with radiation losses. The 1D response is similar to that of Fig. 19 when D is replaced by the equivalence ratio (the turning point defines an intrinsic lean inflammability limit ϕ_{e}), and edge-flame solutions can be constructed via the strategy that we have described. Unexpectedly, however, the edge-speed is positive for all $\phi > \phi_{\mathrm{e}}$, and appears not to vanish in the limit $\phi \searrow \phi_{\mathrm{e}}$ [35].[4] As we shall see, the same kind of thing can happen for the other configurations that we have discussed (both premixed and non-premixed) for certain choices of the Lewis number (or numbers), and we shall discuss the phenomenon in some detail in these other contexts. There, it is linked to the role played by 2D solution branches that can be meaningfully added to responses such as that of Fig. 19, and to edge-flames that link 1D solutions with 2D solutions. Here the matter has not been explored.

[4] Unpublished calculations by Short appear to confirm this behavior.

8. Lifted laminar flames

When a flame supported by the flow from a burner is stabilized at a significant height above the burner rim, it is said to be a lifted flame. A lifted flame propagates in the flow, has an edge unaffected by the burner rim, and for the laminar case at least is stabilized by weak gradients of velocity and mixture strength within the flow. Lifted turbulent flames have long been studied as a framework in which to examine the behavior and properties of non-premixed turbulent combustion, and in recent years it has been recognized that laminar lifted flames can also exist for certain fuels. The first extensive discussion may be found in Ref. [36], and there have been a number of relevant publications by Chung and his colleagues [37–40].

A typical flame-shape is shown in Fig. 22, and has a well-defined annular tribrachial structure, consistent with a high propagation speed (large Damköhler number). The lift-off height z_* is typically much greater than a length characteristic of the flame size, so that apart from a flow displacement in the neighborhood of the flame, the field between the rim and the flame is that of a cold jet with mixing. An examination of this field permits an estimate of the lift-off height, and insight into the stability mechanism. An important parameter is the Schmidt number

$$Sc = \frac{\nu}{D_Y} \tag{73}$$

where ν is the kinematic viscosity, and D_Y is the diffusion coefficient of the fuel supplied by the burner. Stable lifted flames are seen for fuels such as propane and n-butane for which the Schmidt number is greater than 1.

A point force generates a jet with axial velocity

$$u = \frac{3}{8\pi\nu z}\,\frac{J}{\rho}\,\frac{1}{(1+(1/8)\eta^2)^2}, \tag{74}$$

where J is the momentum flux,

$$\eta = \frac{r}{\nu z}\left(\frac{3J}{8\pi\rho}\right)^{1/2}, \tag{75}$$

and z, r are axial and radial coordinates. This is an asymptotically valid description for the jet issuing from a burner when z is large compared to the burner diameter. The corresponding expression for the fuel mass fraction, obtained by solving the species transport equation, is

$$Y = \frac{(1+2Sc)}{8\pi\nu z}\,\frac{I_Y}{\rho}\,\frac{1}{(1+(1/8)\eta^2)^{2Sc}} \tag{76}$$

where I_Y is the supply mass flux of fuel. The oxygen mass fraction is constant.

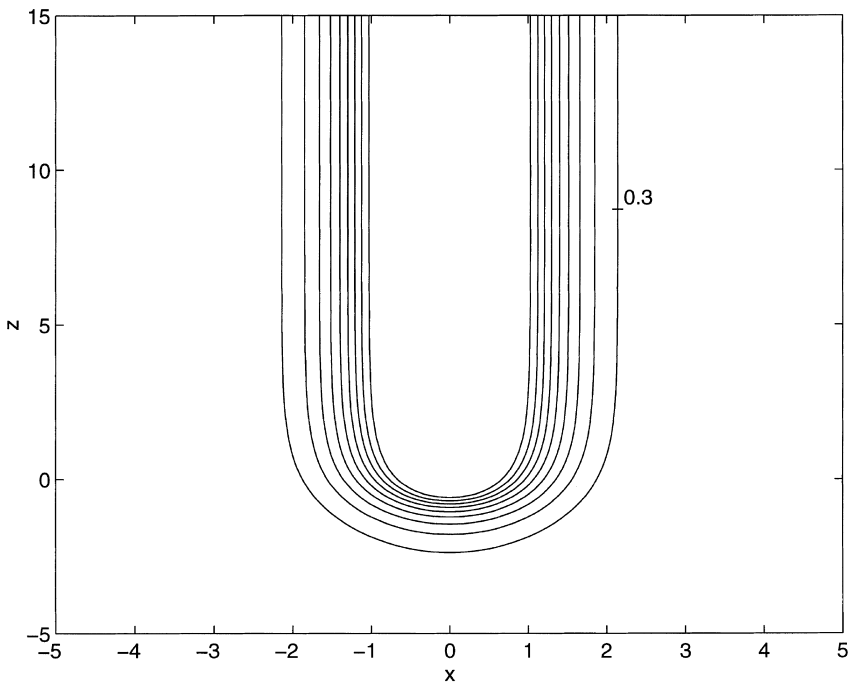

Fig. 21. Temperature contours for an ignition front, twin deflagrations in a symmetric premixed counterflow, from Ref. [35], with permission.

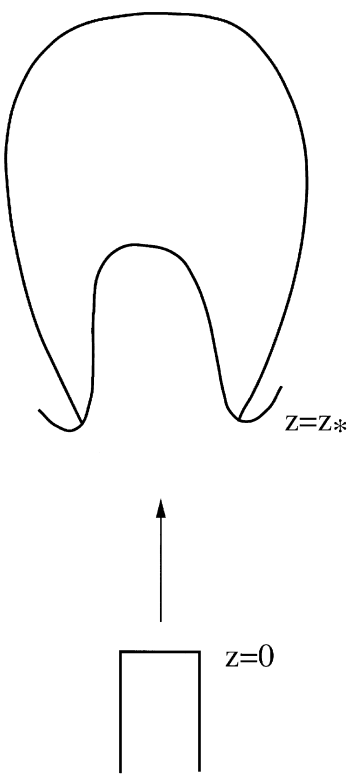

Fig. 22. Schematic of a lifted laminar non-premixed flame.

If we suppose that at the tribrachial ring $z = z_*$, $r = r_*$, the axial velocity is equal to the adiabatic flame-speed for a stoichiometric mixture (the leading term in Dold's estimate of edge-speed for a weakly stretched edge-flame) and Y has the stoichiometric value Y_*, then Eqs. (74)–(76) constitute equations for z_* and r_*, and eliminating r_* we find

$$z_* \sim u_0^{(2Sc-1)/(Sc-1)} \tag{77}$$

where u_0 is a characteristic burner exit speed so that $J \sim u_0^2$ and $I_Y \sim u_0$. Thus the lift-off height increases with blowing velocity if $Sc > 1$ or $Sc < 1/2$. Typical level surfaces $u = u_*$ and $Y = Y_*$ when $Sc > 1$ are drawn in Fig. 23, and where

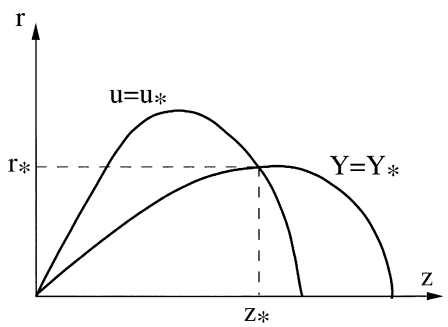

Fig. 23. Level curves $u = u_*$, $Y = Y_*$ for a lifted laminar non-premixed flame.

they cross defines the solution z_*, r_*. If the flow is too strong the curves fail to cross (increasing u_0 increases J more rapidly than I_Y) and blow-off occurs. The curve $Y = Y_*$ defines the stoichiometric level surface, the location of the diffusion flame downstream of the tribrachial ring, and immediately prior to blow-off the flame is located at the tip of this structure with $r_* = 0$.

If the flame is perturbed in a quasi-steady fashion, the tribrachial ring moves along the level surface $Y = Y_*$ so that u changes but the flame-speed u_* does not, and the flame position $z = h$ changes according to

$$\frac{\mathrm{d}h}{\mathrm{d}t} = u - u_* \tag{78}$$

where $u = Ah^{(1/Sc)-1}$ for some constant A. Thus for small perturbations for which

$$h = z_*(1 + z'), \quad |z'| \ll 1, \tag{79}$$

we have

$$z_* \frac{\mathrm{d}z'}{\mathrm{d}t} = Az_*^{(1/Sc)-1}\left(\frac{1}{Sc} - 1\right)z' \tag{80}$$

and this describes a stable (unstable) perturbation if $Sc > 1$ ($Sc < 1$). The Schmidt number for propane is ~ 1.38, that for n-butane ~ 1.52, and stable lifted structures are obtained for these gases. On the other hand, methane and ethane, both of which have Schmidt numbers less than 1, do not exhibit lift-off.

In this discussion it is assumed that the axial gas speed at the tribrachial ring is equal to the adiabatic flame-speed for a stoichiometric mixture. In reality, as the work of Chung et al. recognizes, displacement by the flame of the flow ahead of the flame causes the edge to travel at a speed relative to the undisplaced flow that is greater than it would be in the absence of displacement. This is a hydrodynamic effect lost by the constant density model. The magnitude of the effect depends on the length of the flame, and it is suggested in Ref. [38] that here the effect is a modest one, 30% or so. In the case of mixing layers, for which the flames are long, the effect is much stronger, and analytical evidence is presented in Ref. [41] that for large Damköhler number flames the speed is augmented by a factor $\sim (\rho_\mathrm{f}/\rho_\mathrm{b})^{1/2}$. Numerical results confirm this for density ratios up to ~ 5.

Refinements of the analysis presented here (which follows the work of Chung and his colleagues) that account in an approximate fashion for both stretch effects and flow-divergence effects are described in Ref. [42]. Full DNS of laminar lifted flames, and comparisons with detailed measurements of the combustion field, are reported in Ref. [43].

In the final analysis, laminar lifted flames constitute an exercise in stabilization of a deflagration in non-uniform fields of reactants and velocity, and it is not clear that thinking of them as edge-flames serves much purpose.

9. Effects of edge-curvature

In our discussion so far we have considered only straight edges, and have identified two important Damköhler numbers: D_e, the quenching Damköhler number for the underlying 1D problem; and D_0, the Damköhler number for which the edge-speed is zero. Absent an edge, a flame-sheet can be destroyed by reducing D below D_e; with an edge, it can be destroyed by a failure wave generated when D is reduced below D_0. Particularly in the context of turbulent combustion, flame edges will be curved, and the behavior of a hole in a flame-sheet, or the behavior of an isolated portion of flame (a flame isola) will be affected by the curvature. There has been some discussion of this problem for non-premixed edge-flames.

The effects of curvature on D_0 can be discussed in a cylindrically symmetric context using the 1D model [44]. Then the term $-1/s(\mathrm{d}\theta/\mathrm{d}s)$ is added to the l.h.s. of Eq. (24), V is set equal to zero, and a straightforward analysis yields formulas in terms of modified Bessel functions:

$$\begin{aligned} \Psi_\mathrm{d} &= \frac{I_1(s_*)}{I_0(s_*)} (< 1) \ \text{for a hole}, \\ \Psi_\mathrm{d} &= \frac{K_1(s_*)}{K_0(s_*)} (> 1) \ \text{for an isola}, \end{aligned} \tag{81}$$

where Ψ is defined by Eq. (38) with $D = D_\mathrm{d}$, $\Psi = \Psi_\mathrm{d}$ for a stationary edge ($D_\mathrm{d} = D_0$ and $\Psi_\mathrm{d} = \Psi_0 = 1$ when the stationary edge is straight). Ψ has to be reduced below Ψ_0 to fix the edge of a hole, to prevent it from closing, increased to fix the edge of an isola to prevent it from shrinking, Fig. 24. Thus for fixed D, the edge of a hole is stronger than a straight edge, whereas the edge of an isola is weaker, and the strength and weakness are monotonic functions of curvature. A static stability argument then makes clear that the steady solutions defined by Eq. (81) are unstable: Their significance is as water-shed solutions.

The 1D model has also been used, in a quasi-steady context, to examine edge-speed as a function of Damköhler number and curvature [44], assuming that such a function exists. However, 2D simulations [45] suggest that this can at most be legitimate for a shrinking hole and a shrinking isola. Then trajectories in the edge-speed/radial-location plane are quickly attracted to a universal curve defined by the Damköhler number, independent of the initial radius. On the other hand, for a growing hole or a growing isola, the trajectories only merge after the edge-speed has essentially achieved the infinite radius (straight-edge) value, negative or positive as the case may be. Fig. 25 shows some trajectories for a shrinking hole. The speeds shown are only of qualitative significance, as the fluid displacement effect discussed earlier is not accounted for.

The 2D simulations have also been used to calculate values of D_d for various radii and three fuel Lewis numbers, $Le_Y = 0.5, 1, 1.5$. Le_X is fixed at 1, and the heat of reaction is adjusted for the three cases to fix the Burke–Schumann

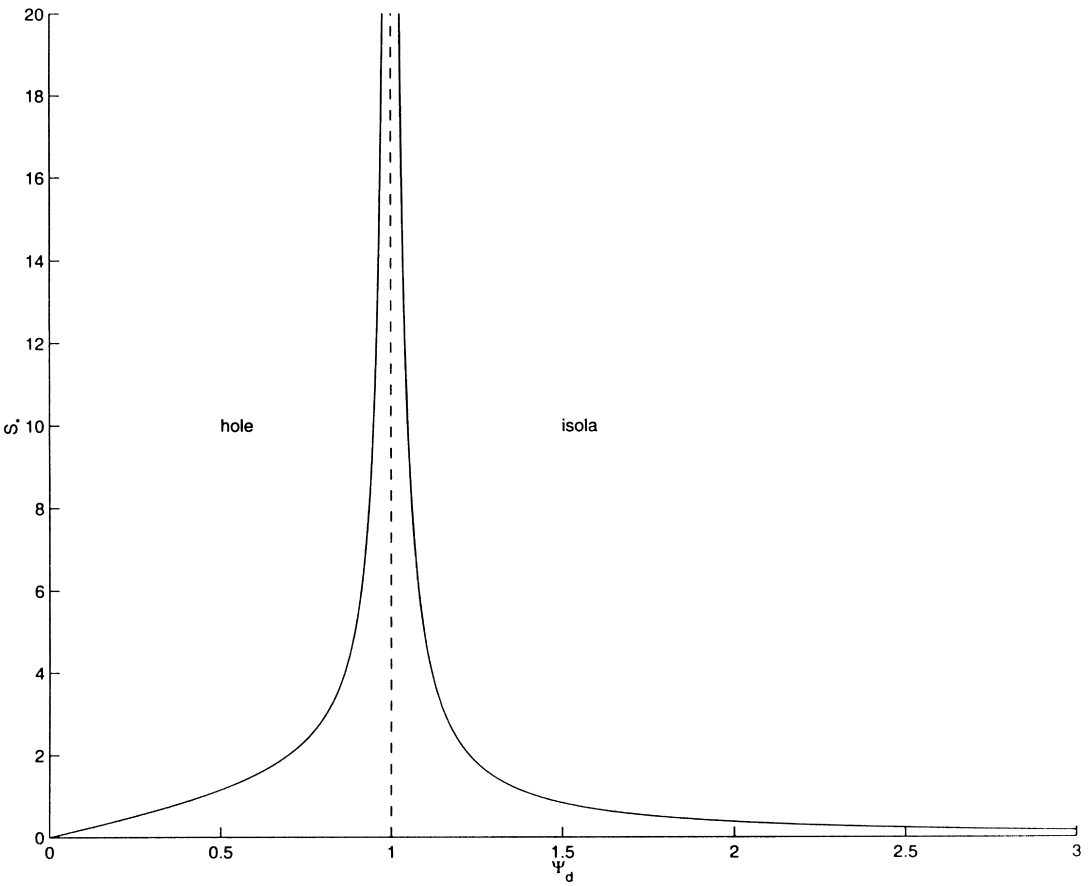

Fig. 24. Variations in the radius of a stationary hole and stationary isola with the scaled Damköhler number Ψ_d, 1D model.

flame-temperature of the underlying 1D problem. Variations of D_d/D_0 with curvature show little variation between the three cases, and D_0 is approximately 70% bigger than D_e in all three cases. The following general remarks may be made: A hole of diameter ~ 1 (the mixing layer thickness) closes for all but a tiny interval of D bounded below by D_e; a hole of diameter ~ 3 closes for D greater than D_e by 30–40%, depending on Le_Y; and a hole of infinite diameter closes for D greater than D_e by more than 70%. Even larger D are required for isolas to grow—thus an isola of diameter less than 1/2 requires a D of at least $2.7 \times D_e$, 50% greater than D_0.

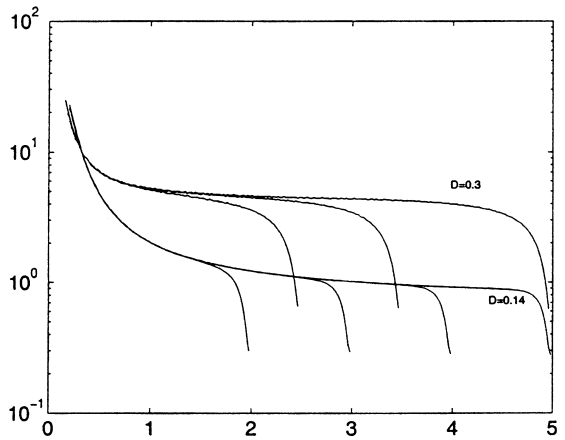

Fig. 25. Trajectories for shrinking holes in the radius-speed plane, from Ref. [45], with permission.

Partially quenched spherical flames have not been discussed, but removal of a small portion generates a hole, removal of most of the flame generates an isola.

9.1. Holes in counterflow flames

The issues of holes in flames and lifted flames come together in experimental observations of Pellet and his coworkers [46]. They examine the axisymmetric counterflow of nitrogen-diluted hydrogen and air and find that at sufficiently small Damköhler numbers a circular hole appears in the single flame-sheet. The computations of Ref. [47] capture this phenomenon and provide an explanation.

At large Damköhler numbers the flame-sheet is whole. Increasing the blowing rate weakens the flame, and at a

critical straining rate extinction occurs at the centerline. But off the axis (on the scale of the jet diameter) where the straining rate (more precisely, the scalar dissipation rate) is lower, the flame can survive in a 1D sense in the mixing layer, and can survive in the absolute sense provided the flame-edge can be stabilized. In the immediate vicinity of the axis the radial velocity is an increasing function of radius, but beyond the jet radius (there is no inert coflow) the velocity is a decreasing function: The edge can be stabilized in this negative gradient. Thus the edge-flame is similar to the lifted flames discussed earlier, as it is stabilized by local field gradients rather than by interaction with a boundary or holder.

10. Thermal-diffusive instabilities

Thermal-diffusive instabilities are a well-known feature of deflagrations and diffusion-flames, and are well understood for both, albeit recently. Roughly speaking, they arise when one or more Lewis numbers are sufficiently small or sufficiently large. Edge-flames are subject to the same instabilities, and we shall start with a discussion in the premixed context.

10.1. Symmetric premixed counterflow, Le = 0.3

Consider the symmetric counterflow of fresh mixture discussed earlier, but now with $Le = 0.3$, a value relevant to lean H_2/air mixtures. This problem was discussed in Ref. [48] where unsteady behavior is accounted for; and in Ref. [49], where steady solutions are discussed (stationary solutions, steadily propagating waves).

The 1D response is similar to that of Fig. 19, where $Le = 1$, except that the maximum temperature is not attained in the limit $D \to \infty$ (zero strain) because of well-known stretch/Lewis number effects, Fig. 26. However, the important distinction between Figs. 19 and 26 is not one of shape, but the stability boundary marked in Fig. 26,

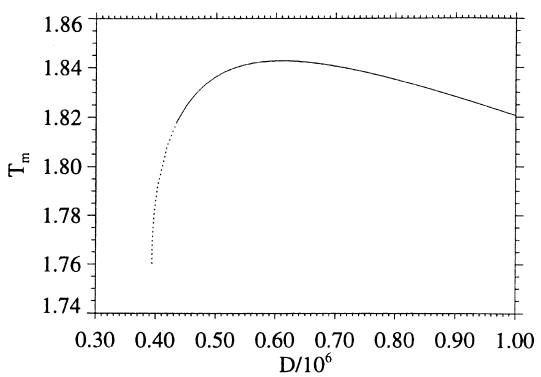

Fig. 26. 1D response for twin symmetric deflagrations in a counterflow, $Le = 0.3$, from Ref. [48], with permission.

associated with Turing instabilities that arise because Le is small. It has long been known that for small values of Le, as here, the unstrained flame displays a cellular instability and that this can be suppressed by a sufficiently large straining flow. Thus some portion of the upper branch extending out to $D \to \infty$ corresponds to unstable solutions. Less well known is the fact that as D is decreased the instability can reemerge as D_e is approached and the twin flames are weakened by their interaction. Thus for values of D in an interval (D_e, D_{NSP}) a linear modal stability analysis, for disturbances $\sim e^{ikz+\lambda t}$, yields real positive eigenvalues for a finite wave-number interval $(k_1(D), k_2(D))$, where $k_1 > 0$ (recall that z is measured perpendicular to the x–y counterflow plane). Linked to this, a branch of steady 2D solutions bifurcates from the point on the upper branch where $D = D_{NSP}$ (the neutral stability point) and wanders in some fashion in the response plane, possibly displaying additional bifurcations and multiplicities. Although its path has not been determined, some part of it lies to the left of $D = D_e$, corresponding to sublimit solutions, as we shall see.

Sublimit solutions, in this sense, are not unusual, are in fact a well-known feature of small Lewis number combustion fields. A good example is afforded by flame-balls, whose spherical geometry makes them robust, better able than a plane flame to resist heat losses or straining flows [50–52]. Flame-balls with radiation losses define an intrinsic inflammability limit that is smaller than the limit ϕ_e for plane solutions. Propagating flames that are cellular can also exist for sublimit conditions, reinforced by the flame front curvature [53]. For the configuration of study here, the sublimit structures have some similarity to flame-balls, but are cylindrical and have been called, in other contexts, flame-strings [54]. Their role in the edge-flame context is that they define the end state {2} when $D < D_{NSP}$, being then the only stable unquenched solution.

Consider first the choice $D = 5.611 \times 10^5$, a value greater than D_{NSP} so that {2} lies on the stable 1D branch. A standard edge-flame is generated in this case, Fig. 27, with an enhanced temperature near the edge, because of the curvature.

The choice $D = 4.031 \times 10^5$ lies in the interval (D_e, D_{NSP}), and the 1D solution is not available as the 'hot' end-point {2}. The computations place {2} on this branch initially, but the instabilities drive it to the 2D branch and the edge leaves behind a train or warp of stationary interacting flame-strings, Fig. 28. The leading cell, advancing unsteadily, elongates and splits in a periodic fashion. The maximum temperature in each trailing string is ≈ 2.1, whereas the minimum temperature on the centerline $x = 0$ is ≈ 0.7, so that each string, although interacting with its neighbors, has a separate identity.

Reduction of D to 3.794×10^5, a value smaller than D_e, leads to different dynamics, Fig. 29. With a cubic interpolation between the quenched solution and the 1D unstable solution for $D = 3.951 \times 10^5$ defining initial

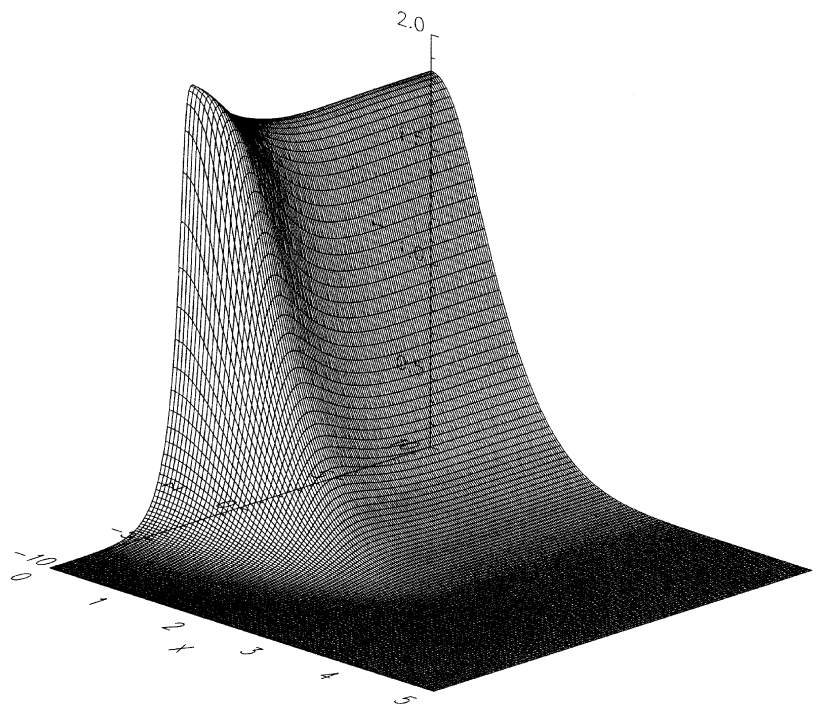

Fig. 27. Temperature topography for an ignition front, twin symmetric deflagrations in a counterflow, $Le = 0.3$, $D = 5.611 \times 10^5$ ($> D_{\mathrm{NSP}}$), from Ref. [48], with permission.

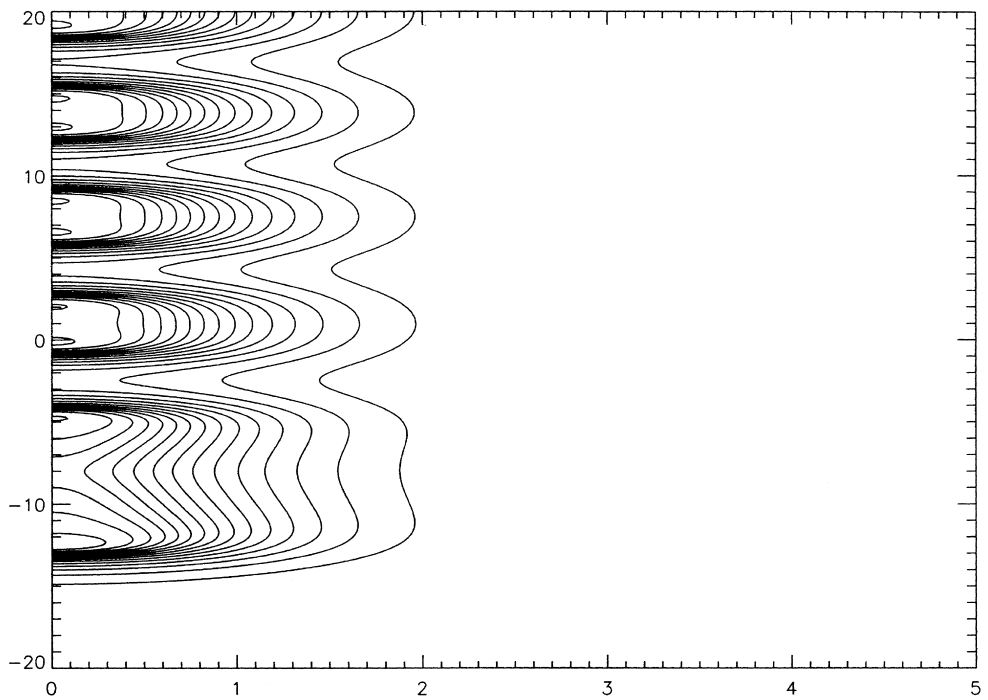

Fig. 28. Temperature contours for an ignition front, twin symmetric deflagrations in a counterflow, $Le = 0.3$, $D = 4.031 \times 10^5$ ($< D_{\mathrm{NSP}}$), from Ref. [48], with permission.

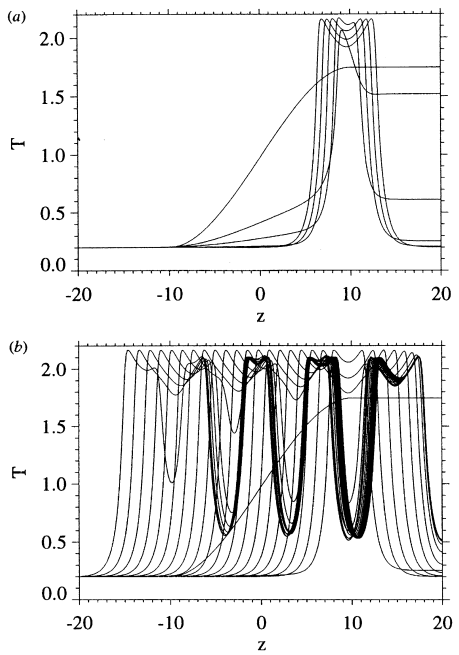

Fig. 29. Unsteady collapse of an edge-flame followed by the advance (right and left) of two ignition fronts, $D = 3.794 \times 10^5$ ($< D_e$), from Ref. [48], with permission.

conditions, the edge advances but the post-edge structure collapses. The surviving edge structure then acts as an ignition source for propagation in both directions, with one edge advancing in the positive z-direction, the other in the negative z-direction. The widening structure between the edges is a line of stationary interacting flame-strings.

Steady edge-speeds, where they are defined (no trailing cellular structures) are shown as a function of the rate of strain for various Lewis numbers in Fig. 6 of Ref. [49] which we do not reproduce here as it is qualitatively very similar to Fig. 33 which shows edge-speeds for the non-premixed case, discussed in Section 11.

Other types of solution are possible and what is

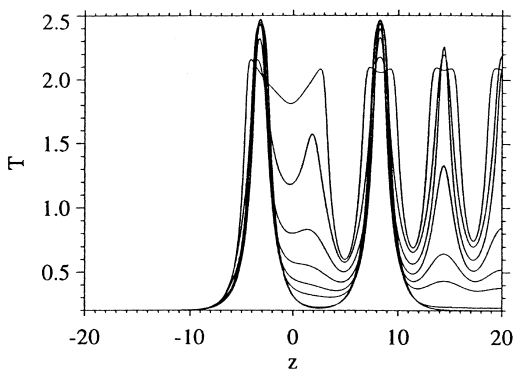

Fig. 30. Temperature profiles at the symmetry plane: evolution to twin stationary flame-strings, $D = 1.343 \times 10^5$, from Ref. [48], with permission.

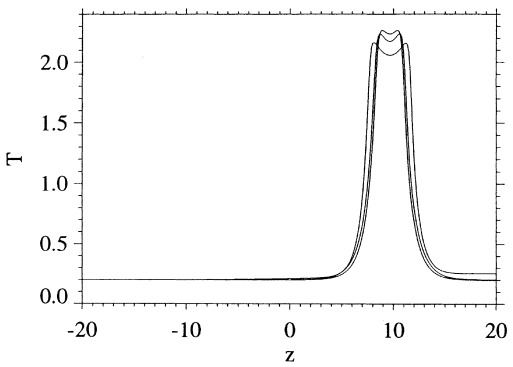

Fig. 31. Temperature profiles at the symmetry plane: evolution to a single flame-string, $D = 1.976 \times 10^5$, from Ref. [48], with permission.

generated in the long time depends on the choice of D and on the initial conditions. Fig. 30 shows a pair of stationary strings generated when $D = 1.343 \times 10^5$. Here the post-edge structure collapses, but the surviving structure fails to act as an ignition source and a short flame survives with two stationary edges. Fig. 31, $D = 1.976 \times 10^5$, is a variation on this, a single stationary string.

A large number of calculations for $D < D_{NSP}$ lead only to the three late time configurations described here—an 'infinite' chain of strings, a pair, or a singleton. These are also the only configurations observed in Ronney's experiments, which we discuss later; photographs of a string pair and a single string are reproduced in Fig. 32 [55].

The phenomena that we have described in this section only occur for values of Le which are rarely met, absent artificial mixture additives (SF_6, for example). When $Le = 0.7$, and $D \approx D_e(Le)$ (the Lewis number-dependent extinction Damköhler number) but larger, the edge-speed is negative and sublimit structures do not exist, although they do for $Le = 0.5$. Thus the only common mixture in which these things will be seen is lean hydrogen/air.

11. Lewis number effects and the counterflow diffusion edge-flame

It has long been known that diffusion flames can display cellular instabilities for suitable choices of the Lewis number, and recent work has substantially clarified the matter [56,57]. The instabilities occur in a neighborhood of the extinction point (e.g. the neighborhood of $D = D_e$ in Fig. 2). Thus, phenomena similar to that which we have described in Section 10 can occur in the diffusion flame context.

An extensive discussion of non-premixed edge-flames with $Le_X = 1$ and various values of Le_Y can be found in Ref. [28]. The propagation speeds of weakly stretched (large D) tribrachial flames are calculated using asymptotic methods (cf. Eq. (60) for $Le_X = Le_Y = 1$), and numerical solutions

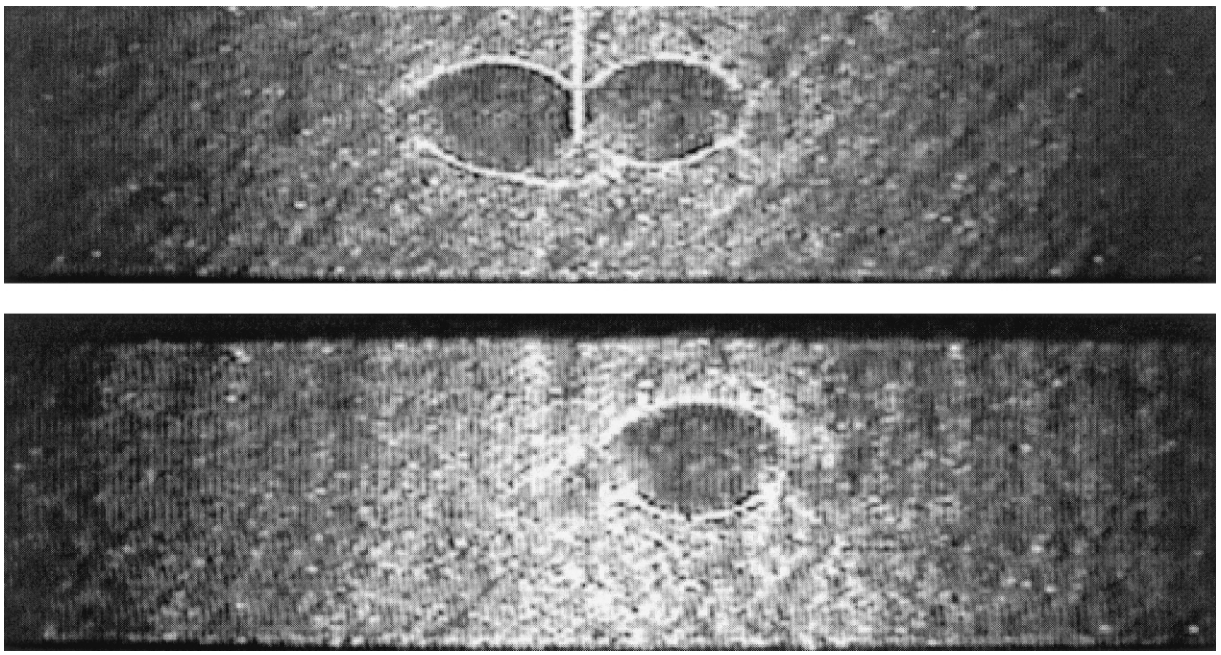

Fig. 32. Flame-string structures (pair and singleton) observed experimentally in the symmetric twin counterflow configuration for lean hydrogen/air mixtures, from Ref. [55], with permission.

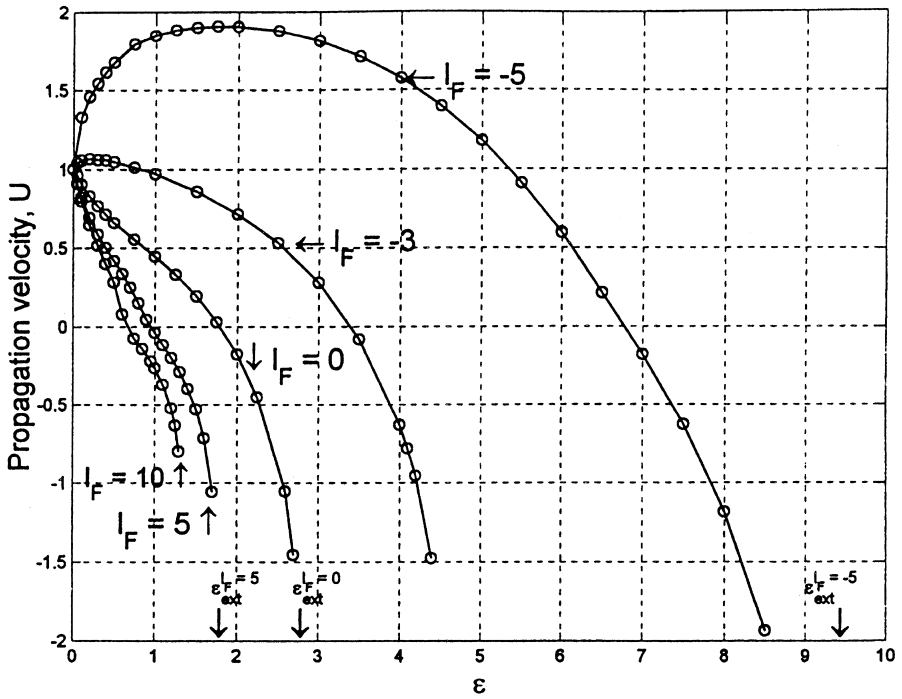

Fig. 33. U/S_o vs. rate of strain for edge-flames in a non-premixed counterflow, showing the effect of Lewis number, from Ref. [28], with permission; l_F is negative for $Le_Y < 1$, positive for $Le_Y > 1$. Note that edge-speeds calculated using the constant-density model are subject to serious error, because of failure to account for the displacement effect discussed in Section 8. It is conceivable, therefore, that some of the qualitative features identified here could be in error.

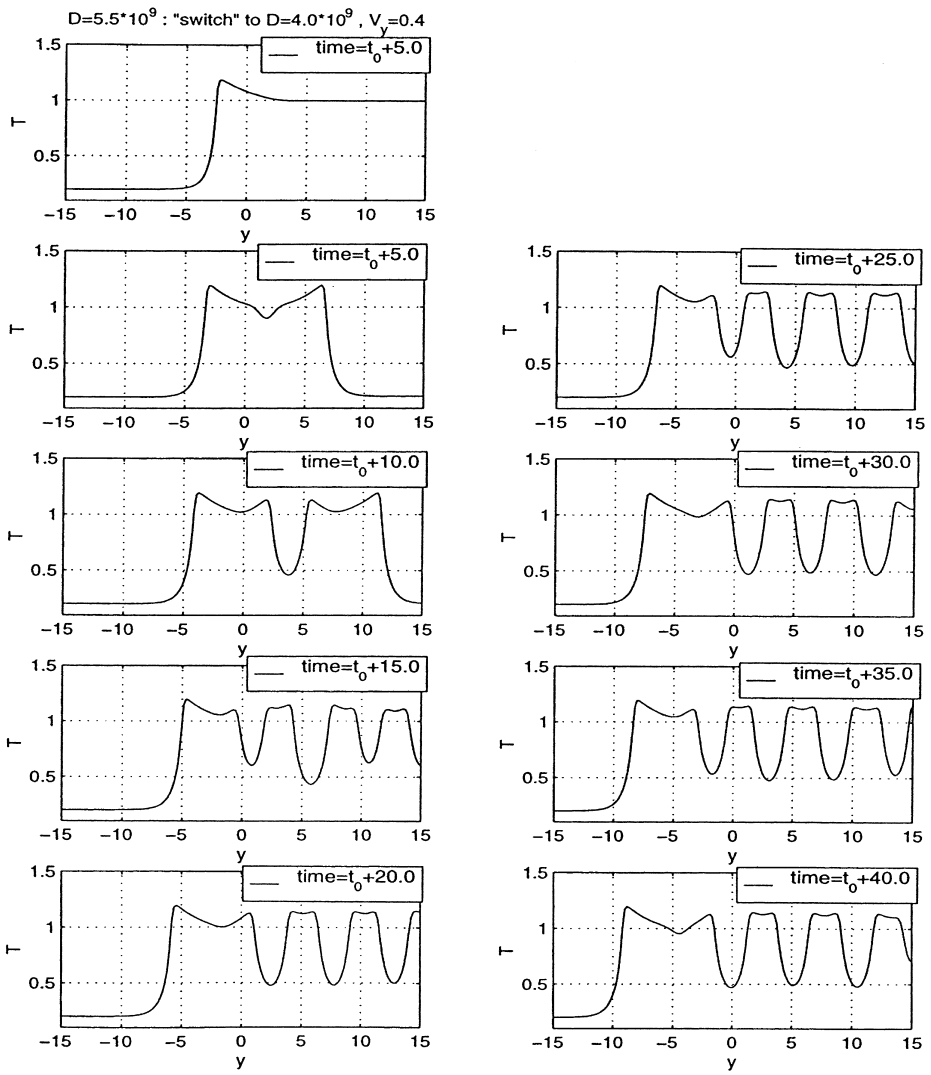

Fig. 34. The periodic structure (cellular) generated by an ignition front at a sub-ignition Damköhler number, non-premixed, $Le_Y = 0.3$, $Le_X = 0.3$, from Ref. [60], with permission. (In the present notation, y would be replaced by z.)

are constructed when D is not large, Fig. 33. This figure looks quite similar to Fig. 4.4 of Ref. [58] which shows variations of flame-speed with rate of strain for a 1D deflagration in a counterflow. (As we noted earlier, flame-speed can only be legitimately defined for a weakly stretched deflagration; for an unbounded edge-flame however, which propagates in a wave-like fashion, edge-speed is meaningful even if a leading deflagration is strongly stretched.)

Interestingly, the calculations of Ref. [28] do not lead to cellular structures for small Le_Y. The reason for this is that diffusion-flame instability depends critically not on just the choice of Lewis numbers, but also on an equivalence ratio defined as the ratio of the mass fraction of fuel in the fuel supply to the mass fraction of oxidizer in the oxidizer supply, normalized with the stoichiometric ratio. This has to be sufficiently small to generate cellular instabilities when Le_Y is small, but the calculations of Ref. [28] are for a value of 1. This point is discussed further in Section 11.1.

When both Lewis numbers are small, cellular instabilities can be generated without concerns about the supply stoichiometry, and studies have been made of the symmetric counterflow for $Le_X = Le_Y = 0.3$. Solutions exhibit sublimit structures (solutions for $D < D_e$), a positive edge-speed when $D = D_e$, and edge-flames that correspond to a transition between a stable 1D solution and a stable 2D (cellular) solution. This problem was first discussed by Thatcher and Dold in an unpublished report of the Seventh International Conference on Numerical Combustion,

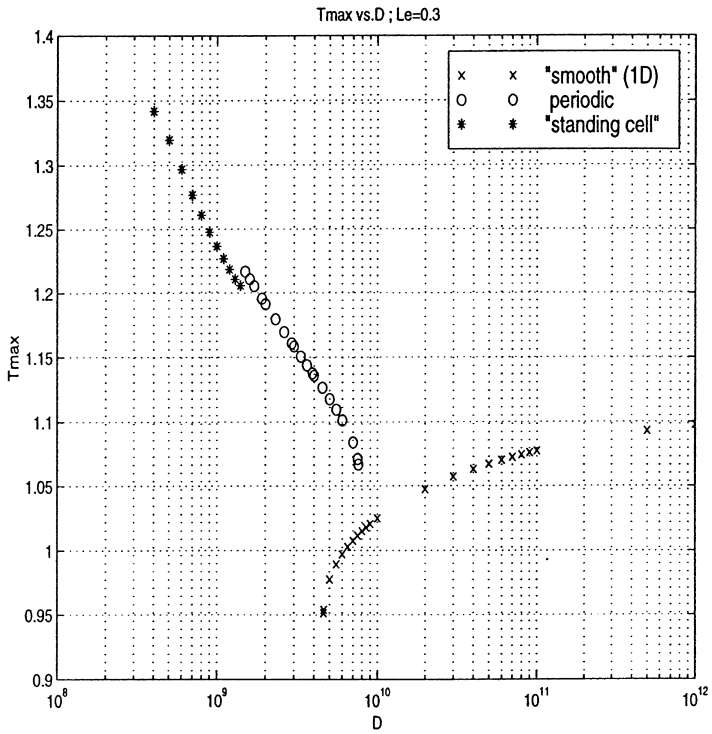

Fig. 35. Maximum temperature vs. Damköhler number on a number of solution branches, non-premixed, $Le_Y = 0.3$, $Le_X = 0.3$, from Ref. [60], with permission: (×) 1D; (○) periodic array of strings; (∗) single string.

1998, work that was eventually published in Ref. [59], but we shall present results from the Masters thesis of Kochevets [60].

Thus consider the problem

$$\left(\frac{\partial}{\partial t} - x\frac{\partial}{\partial x}\right)(T, Y) = \left(\frac{\partial^2}{\partial x^2} + \frac{\partial^2}{\partial z^2}\right)\left(T, \frac{1}{Le}Y\right) + DY(Y - \Phi)\mathrm{e}^{-\theta/T}(1, -1),$$

$$\Phi = Y - X = \mathrm{erf}\left(x\sqrt{\frac{Le}{2}}\right), \tag{82}$$

$$x \to -\infty : T \to T_\infty,\ Y \to 0;$$

$$x \to +\infty : T \to T_\infty,\ Y \to 1;$$

$$|z| \to \infty : \frac{\partial T}{\partial x} = 0 = \frac{\partial Y}{\partial z}.$$

Note the use of Neumann data as $|z| \to \infty$; the desired solutions are generated by appropriate choice of the initial conditions. The parameters are $Le = 0.3$, $T_\infty = 0.2$, $\theta = 15$, $T_{\mathrm{bs}} = 1.1128$, and the extinction Damköhler number is $D_{\mathrm{e}} = 4.55 \times 10^9$ with a corresponding maximum temperature $T_{\max} = 0.95$.

Edge-flames generated in this way have positive edge-speeds for $D \geq D_{\mathrm{e}}$, and also for an interval to the left of D_{e}. Consider, for example, what happens when $D = 5.5 \times 10^9$ is used to define initial conditions, but at $t = 0$, D is reduced to the value 4×10^9. The post-edge state collapses but the edge survives, Fig. 34, and acts as an ignition source for two fronts, one traveling to the left, the other to the right, just as in Fig. 29 for the twin deflagrations.

Two kinds of sublimit structures are reported, a periodic array of cells or flame-string like structures, or a single flame-string. These solutions are constructed using periodic boundary conditions in z in an attempt to accurately establish the late time configuration, free of influence from initial conditions. Since the period of the periodic array is not known a priori, the computation interval is adjusted until an integer number of identical cells occupy the interval in late time. In this way it is possible to calculate a portion of the 2D solution branch that, it is inferred, bifurcates from the strong-burning 1D branch.

Thus Fig. 35 shows three sets of points in the $T_{\max}-D$ plane. The crosses lie on the 1D response, asymptoting to the Burke–Schumann temperature of 1.1128, and terminating at D_{e} where $T_{\max} = 0.95$. The circles represent solutions characterized by a periodic array of cells. The curve so traced appears to have a vertical tangent at $D \approx 7.5 \times 10^9$ below which solutions are not found, suggesting the existence of an unstable branch that bifurcates subcritically from the 1D branch. The stars represent single cell solutions. It is not possible to construct anything but quenched

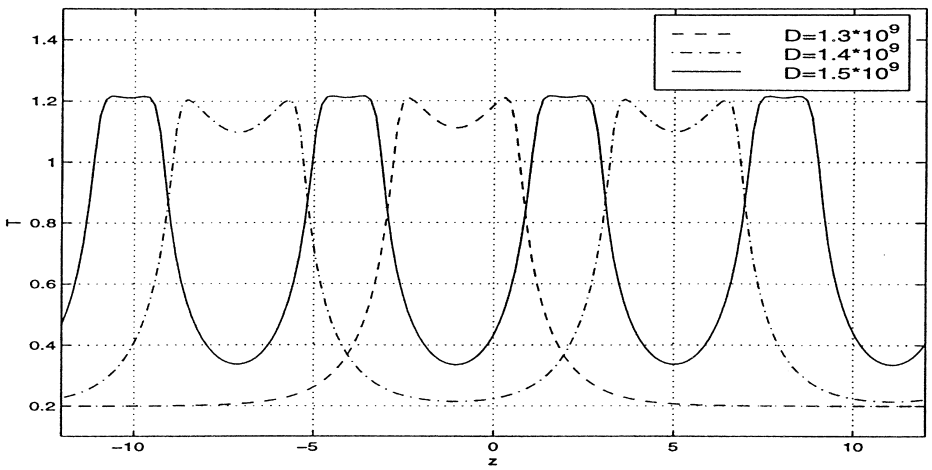

Fig. 36. Solution in the neighborhood of the transition from the single string branch to the periodic string branch of Fig. 35, from Ref. [60], with permission.

solutions for values of D less than approximately 4×10^8. And there is evidence of complicated behavior in the neighborhood of $D=1.4\times10^9$ at the end of the single cell branch and the periodic cell branch. Fig. 36 shows solutions for three values of D. For the smallest value, 1.3×10^9, the solution is characterized by a single cell, and for the largest value, 1.5×10^9, it is characterized by an array of cells whose period is consistent with the neighboring solutions on the periodic branch. But for the intermediate value $D=1.4\times10^9$ a periodic solution is generated with a period roughly double that for the larger D.

11.1. The counterflow diffusion flame, $Le_X=1$, $Le_Y=0.3$

So far we have discussed diffusion-flame edges when $Le_X=Le_Y=0.3$. These values can be generated in the laboratory by appropriate choice of reactants and diluents, but diluted hydrogen burning in air is of more practical importance, and we discuss it here [61].

Now the problem is

$$\left(\frac{\partial}{\partial t}-x\frac{\partial}{\partial x}\right)(T,X,Y)=\left(\frac{\partial^2}{\partial x^2}+\frac{\partial^2}{\partial z^2}\right)\left(T,X,\frac{1}{Le_Y}Y\right)+(q,-\alpha_X Y_\infty,-\alpha_Y X_\infty)DXY\,\mathrm{e}^{-\theta/T},\tag{83}$$

$$x\to-\infty: X\to1,\ Y\to0,\ T\to T_\infty;$$

$$x\to+\infty: X\to0,\ Y\to1,\ T\to T_\infty;$$

$$|z|\to\infty: \frac{\partial}{\partial z}(\cdot)\to0.$$

Here X and Y have been scaled with the supply values X_∞ and Y_∞, so that the modified stoichiometric coefficients are $\alpha_X Y_\infty$ and $\alpha_Y X_\infty$, and the ratio

$$\eta=\frac{\alpha_X Y_\infty}{\alpha_Y X_\infty}\tag{84}$$

plays an important role in the nature of the solutions, controlling, along with Le_Y, whether or not cellular structures are generated. (The significance of η is emphasized in Ref. [57] for cellular instabilities of 1D flames , in Ref. [62] for pulsating instabilities of 1D flames.) If $\alpha_X/\alpha_Y=8$, corresponding to the global reaction

$$H_2+\tfrac{1}{2}O_2\to H_2O,$$

and $X_\infty=0.22$ (air), $Y_\infty=0.01$ (14% hydrogen in nitrogen), then $\eta=0.36$. Cellular structures can be generated for this case (and also for $\eta=0.5, 0.75$), but not for $\eta=1$.

The 1D extinction Damköhler number is 1.837×10^5, but solutions can be found for D as small as 1.2×10^5. The strong-burning 1D solution is marginally stable when $D=1.897\times10^5$, but DNS yield cellular structures, implying a subcritical bifurcation from the neutral stability point. The concentration contours for the stationary array of strings generated when $D=1.89686\times10^5$ shown in Fig. 37 give some insights into the nature of the combustion field in this case. At the center of each string (where the contours are vertical) there are x-wise fluxes of fuel (to the left) and oxidizer (to the right) corresponding to a diffusion flame. However, there is substantial mixing between each string, and mixed fluxes from these regions move with a substantial z-component to sustain reaction within the string.

A finite number of strings can be generated (sublimit structures) and three are reported when $D=1.28427\times10^5$, two for $D=1.22499\times10^5$, and one for $D=1.18548\times10^5$. These structures are sustained because Le_Y is small, and we expect Le_Y to be most relevant in fuel-lean regions of the combustion field, where $X/Y>0.36$ (recall that X and Y have both been scaled with supply values). But it is probable

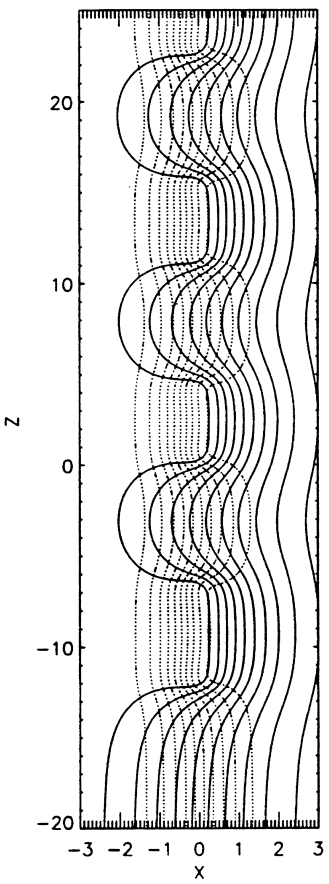

Fig. 37. Fuel (solid) and oxydizer (dotted) concentration contours for a stationary array of strings generated by the counterflow of diluted hydrogen with air, $D = 1.89686 \times 10^5$, from Ref. [61], with permission.

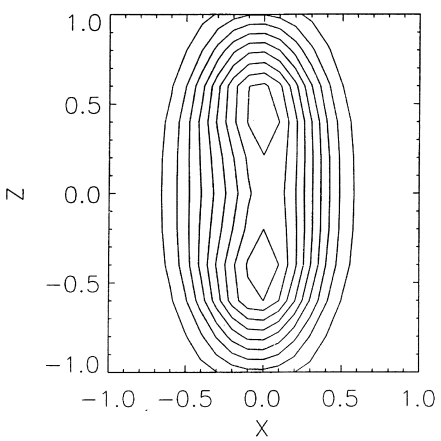

Fig. 38. Reaction-rate contours for a single string in a two-string configuration, $D = 122,499$, from Ref. [61], with permission.

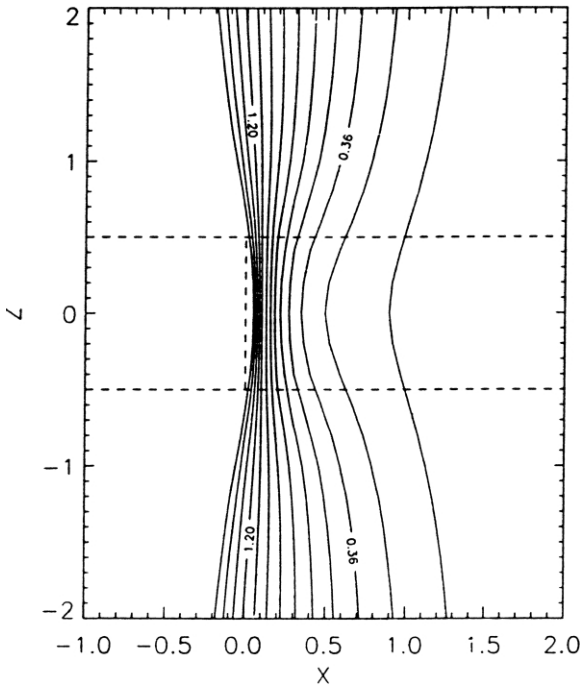

Fig. 39. Contours of X/Y corresponding to Fig. 38. The intersection of the broken lines identifies the locations of the reaction-rate maxima, and these lie on the fuel-lean side of $X/Y = 1.2$, from Ref. [61], with permission.

that this is not sufficient. For an isolated flame-ball, the shift from fuel-lean to fuel-rich combustion occurs not when X_∞ and Y_∞ are in stoichiometric proportion, but when $Le_X^{-1}X_\infty$ and $Le_Y^{-1}Y_\infty$ are in stoichiometric proportion since, in the final analysis, it is the fluxes to the reaction zone that matter, and for a flame-ball these are entirely diffusional [51,63]. If we apply that criterion here, viz. $Le_X^{-1}X/Le_Y^{-1}Y = 0.36$, then $X/Y = 1.2$ and indeed, the reaction rate maxima for a string lie on the lean side of the contour, Figs. 38 and 39.

The sublimit structures that can be generated in a plane counterflow, whether premixed or non-premixed, are cylindrical in nature. More generally, and specifically in the case of a turbulent flow, we might expect to see an ensemble of flame-balls, the spherical or near-spherical counterparts. The implications for turbulent modeling of lean hydrogen flames are clear: classical laminar flamelet concepts must be modified to account for the ability of the burning structures to adopt highly curved forms which resist quenching.

12. Oscillating edges

Oscillating edge-flames in which the edge advances and retreats have long been observed in a number of experimental configurations. For example, when a flame spreads over a liquid fuel-bed, Fig. 1a, the speed U with which the

flame advances is usually a constant, U_o say. But there are circumstances in which U fluctuates with time, viz.

$$U = U_o + U'(t)$$

where U' is periodic. The oscillations are notably non-linear and each period of oscillation is characterized by long intervals of modest motion (U' small) punctuated by bursts of rapid advance (U' large). It has long been believed that during the 'rest' phase the flame is essentially a diffusion flame, whereas during the advance it has the characteristics of a deflagration. The oscillations occur under *reduced flame-strength conditions*, a reduction obtained, for example, by lowering the liquid pool temperature so that the vigor of the evaporation is reduced.

Edge-flame oscillations are also seen in other flame configurations. The microgravity candle flame, Fig. 1b, oscillates prior to extinction, extinction brought about by a growing oxygen deficiency through confinement. The edge retreats and advances with negligible side movement of the flame-sheet, the oscillation growing in amplitude until the flame is pinched off at the top. Five oscillations or so were seen in the Shuttle experiments, 90 or so in the Mir experiments, presumably a result of different confinement volumes.

Oscillations are also seen in the configuration of Fig. 1g when conditions are close to blow-off [8,9]. Also, if PMMA cylinders are burnt in a convective flux of air, extinction at the front stagnation point (a local stretch effect) creates twin flame edges which retreat and advance several times [64].

In the context of flame-spread over liquids, this phenomena has been captured in numerical simulations, and various explanations have been proposed. One links the oscillations to a gas-phase eddy [65]; the other to Marangoni instabilities [66]. We shall not discuss them here since they have more to do with flame-spread[5] than edge-flames, but it seems likely that at least for the oscillations observed in flame spread when the atmospheric nitrogen is replaced by helium [1] the Lewis number mechanism that we shall describe in this section is the likely cause, as no oscillations of the liquid are observed.

We shall discuss a model, proposed in Ref. [70], which contains ingredients common to all the configurations in which oscillations are observed, and we shall describe oscillating solutions admitted by this model.

All of the configurations have two common characteristics: near limit combustion, and fuel Lewis numbers significantly greater than 1. (We have the estimates $Le_{\text{fuel}} \approx 1.5$ for a flame spreading over propanol, $Le_{\text{fuel}} \approx 2.5$ for candle vapors, $Le_{\text{fuel}} \approx 1.6$ for PMMA vapors, $Le_{\text{fuel}} \approx 1.4$ for ethane, and $Le_{\text{fuel}} \approx 1.3$ for methanol.) Furthermore, in all of the configurations the flame-edge is, in some sense, anchored. For the candle flame the base of the wick marks the end of the vapor source, and so is an anchor point. For the problem of fuel injection through a plate the upstream edge of the injection region defines an anchor. For a flame spreading over liquid the flame creates its own anchor at the leading edge, constrained by the heat transfer/evaporation processes which generate the fuel vapor. (There is no anchor for propagation above the flash-point.)

The model contains all three characteristics, and they are probably necessary for the generation of oscillating solutions, although a definitive claim would be unwise. Certainly the counterflow diffusion flame can be weakened by reducing D, and a large fuel Lewis number can be adopted, but these choices merely lead to a rapid retreat of the edge as a failure wave and, as we shall see, negative edge-speeds tend to suppress oscillations. By anchoring a flame, negative edge-speeds can be prevented prior to blow-off or detachment.

The model configuration is sketched in Fig. 40 and consists of an oxygen-supply boundary at $x = -(1/2)$, $-\infty < z < +\infty$, and a fuel-supply boundary at $x = +(1/2)$, $0 < z < +\infty$. The remainder of the upper wall ($x = +(1/2)$, $-\infty < z < 0$) supplies neither oxygen nor fuel, although it can be a sink of both since Dirichlet data are used, rather than flux conditions. The point $z = 0$, $x = +(1/2)$ corresponds to a soft anchor, an attachment point for a flame that lies nominally in $z \geq 0$. It is less constraining than a hard anchor (e.g. a cold splitter plate on the line $x = 0$, $z < 0$), in the spirit of the experimental anchors.

The combustion field within the walls is governed by the

[5] The problem of flame-spread has been extensively studied, both theoretically and experimentally. The review of Wichman [67] is a fine discussion of the early history of the problem for a solid fuel-bed, starting essentially with the thesis of deRis [68]. The slightly later review by Ross [1] for a liquid fuel-bed brings up to date an earlier review by Glassman and Drier [69]. Much has been learnt over the past 30 years, particularly since the inception of microgravity studies.

An essential characteristic of flame spread, whether it occurs over a solid or over a liquid whose temperature is below the flash-point temperature is that heat generated at the flame is carried ahead of the flame by various mechanisms, heats the bed, and thereby generates the gaseous fuel necessary to support (with the surrounding atmosphere) what is, in nominal terms, a diffusion flame. The flux of heat can arise from one or more of the following mechanisms: gas-phase conduction, condensed-phase conduction, gas-phase convection, liquid-phase convection, radiation. Marangoni forces play an important role in the liquid convection.

The forward portion of the diffusion flame, near the surface, is quenched; there is a dead space between the surface and the region where chemical reaction is first significant. Thus the flame has an edge, and this edge structure can display some of the characteristics of edge-flames. As long ago as 1968 deRis [68] argued that the edge-structure should be tribrachial in nature, although in his famous analysis of the spread problem, this feature is suppressed by the core approximations. It is now well recognized that the details of the combustion field in the neighborhood of the edge play a crucial role in determining the spread rate.

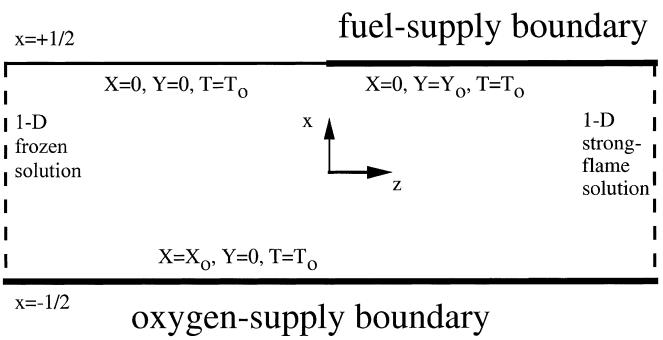

Fig. 40. The model configuration used for the investigation of oscillating edge-flames.

equations

$$\left(\frac{\partial}{\partial t}+V\frac{\partial}{\partial z}\right)=\nabla^2\left(X,\frac{Y}{Le_Y},T\right)+\left(-\frac{1}{2},-\frac{1}{2},1\right)DXY\,\mathrm{e}^{-\theta/T}, \tag{85}$$

where it is assumed that $Le_X = 1$. V is the speed of an applied convective flow in the z-direction.

These equations have a 1D (x-dependent) solution, multivalued provided the activation energy θ is large enough. The weak solution, assuming reaction is negligible at the temperature T_o, is

$$X = X_o\left(\tfrac{1}{2}-x\right), \qquad Y=0, \qquad T=T_o. \tag{86}$$

The strong solution can only be constructed numerically, but its fast-chemistry ($D\to\infty$) approximation is

$$\begin{aligned}
&-\frac{1}{2}<x<x_*: X=\frac{X_o(x_*-x)}{\left(\frac{1}{2}+x_*\right)},\ Y=0,\\
&T-T_{bs}=-(T_{bs}-T_o)\frac{(x_*-x)}{\left(\frac{1}{2}+x_*\right)};\\
&x_*<x<\frac{1}{2}: X=0,\ Y=\frac{Y_o(x-x_*)}{\left(\frac{1}{2}-x_*\right)},\\
&T-T_{bs}=-(T_{bs}-T_o)\frac{(x-x_*)}{\left(\frac{1}{2}-x_*\right)};
\end{aligned} \tag{87}$$

where

$$x_*=\frac{0.5(X_oLe_Y-Y_o)}{(Y_o+X_oLe_Y)} \tag{88}$$

is the flame-sheet location, and

$$T_{bs}=T_o+\frac{2X_oY_o}{Y_o+X_oLe_Y} \tag{89}$$

is the flame-temperature. The frozen solution (86) provides boundary conditions at the left computational boundary, and the Burke–Schumann solution (87)–(89) provides an approximation to the boundary conditions at the right computational boundary. The exact conditions at the hot boundary are obtained numerically, and only exist if D is greater than a 1D quenching value D_e that is Lewis number-dependent. Fixed parameter values are $X_o = Y_o = 1$, $T_o = 0.15385$.

12.1. Results

Consider first the choice $V = 0$, $Le_Y = 1.8$, for various values of D. Fig. 41 shows the 1D (hot-boundary) response, with $D_e \approx 0.55\times10^7$, defining the S(tatic) Q(uenching) P(oint). A second Damköhler number of significance, also marked on the figure, is $D_{NSP} \approx 1.01\times10^7$, the 2D (edge-flame) stability boundary. For $D > D_{NSP}$, solution of the 2D problem leads, following initial transients, to a stationary edge-flame, but for an interval $D_{DQP} < D < D_{NSP}$ ($D_{DQP} \approx 0.875\times10^7$) oscillating (limit cycle) solutions are generated, which also define points in the response. Fig. 42 shows time variations of T at $z = 0.75$, $x = 0.08$ for various values

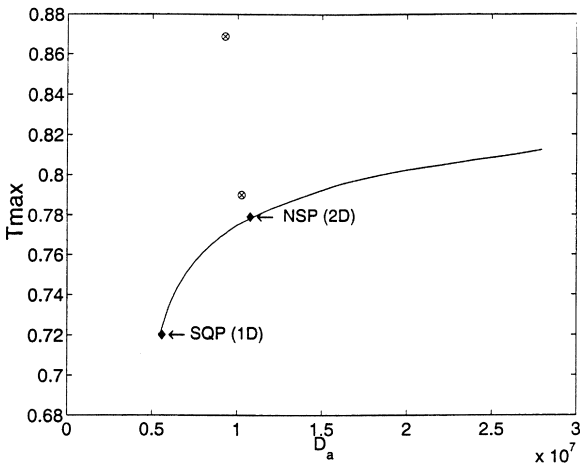

Fig. 41. Response for $Le_Y = 1.8$, $U = 0$. SQP is the static quenching point defining what elsewhere we label D_e; NSP is the neutral stability point for the edge-flame oscillations: (—) 1D response; ($*$) 2D oscillating solutions, from Ref. [71], with permission.

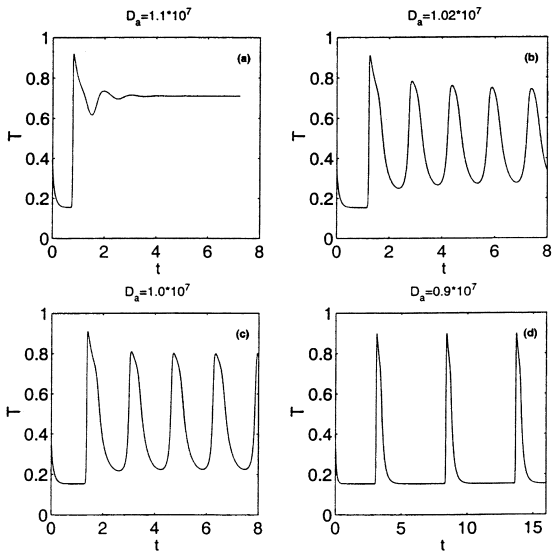

Fig. 42. Temperature history at $z = 0.75$, $x = 0.08$ for $Le_Y = 1.8$, $U = 0$, $D = 1.1 \times 10^7$, 1.02×10^7, 1.0×10^7, 0.9×10^7, from Ref. [71], with permission.

of D, two of them greater than D_{NSP}, two less. The fourth panel, for $D = 0.9 \times 10^7$, hints at an extensive rest phase interrupted by a sharp excursion during each period, and this becomes clear when the flame position and speed are plotted against time. This is done in Fig. 43 for slightly different parameter values ($Le_Y = 2, D = 1.6 \times 10^7$), over a complete period. The edge drifts slowly backwards in the interval (2,4), advances rapidly in the interval (4,4.4), and then again retreats slowly. During the retreat the structure is that of a rounded diffusion flame-sheet, with maximum reaction rate 18 or so, Fig. 44. But during the advance the edge is characterized by a tribrachial structure with a maximum reaction rate greater than 100, Fig. 45.

Returning to the response of Fig. 41, when D is reduced below D_{DQP} the 2D solution fails, and the flame retreats to the hot boundary where it only survives because the boundary is an ignition point. D_{DQP} is a dynamic quenching point for the 2D solution.

The important role of the Lewis number is revealed by examining the case $U = 0$, $Le_Y = 1.5$. Here $D_{\mathrm{SQP}} \approx 0.25 \times 10^7$. No instabilities are seen for any D, but there is a critical value $D_{\mathrm{IDP}} \approx 0.48 \times 10^7$, below which failure occurs and the flame detaches from the anchor, retreating to the hot boundary.

The following general conclusions can be drawn. A reduction in the Damköhler number weakens the 1D (hot-boundary) flame, eventually extinguishing it, but the 2D edge-flame is more vulnerable and is extinguished earlier. Provided the Lewis number is large enough, the edge-flame displays sustained oscillations for Damköhler numbers close to the quenching value.

12.2. Effects of V

We turn now to the effects of the convective flux in the

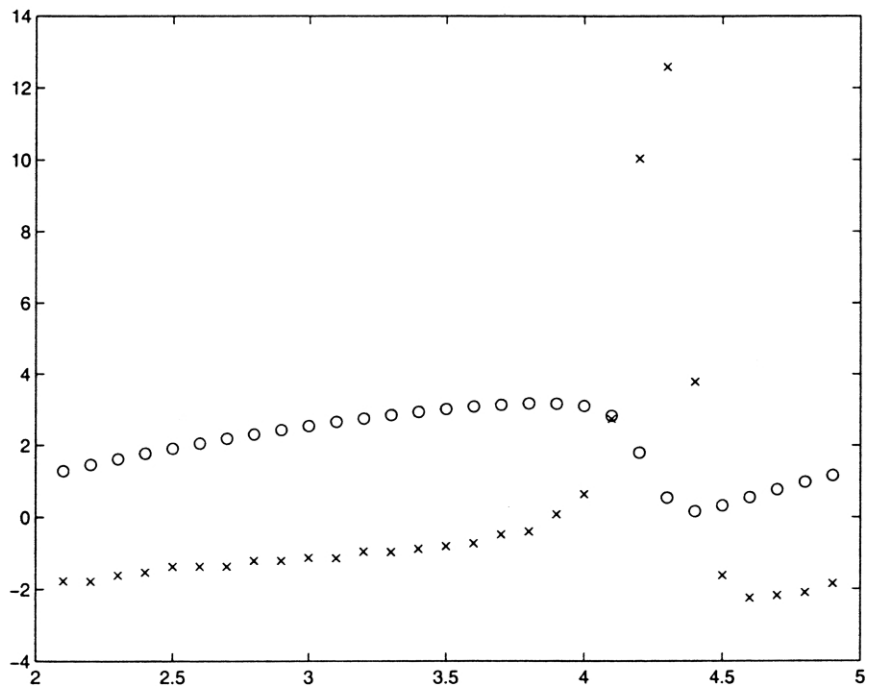

Fig. 43. The front position (○) and approximate speed (×) in the time interval [2.1,4.9], $Le_Y = 2$, $D = 1.6 \times 10^7$, from Ref. [70], with permission.

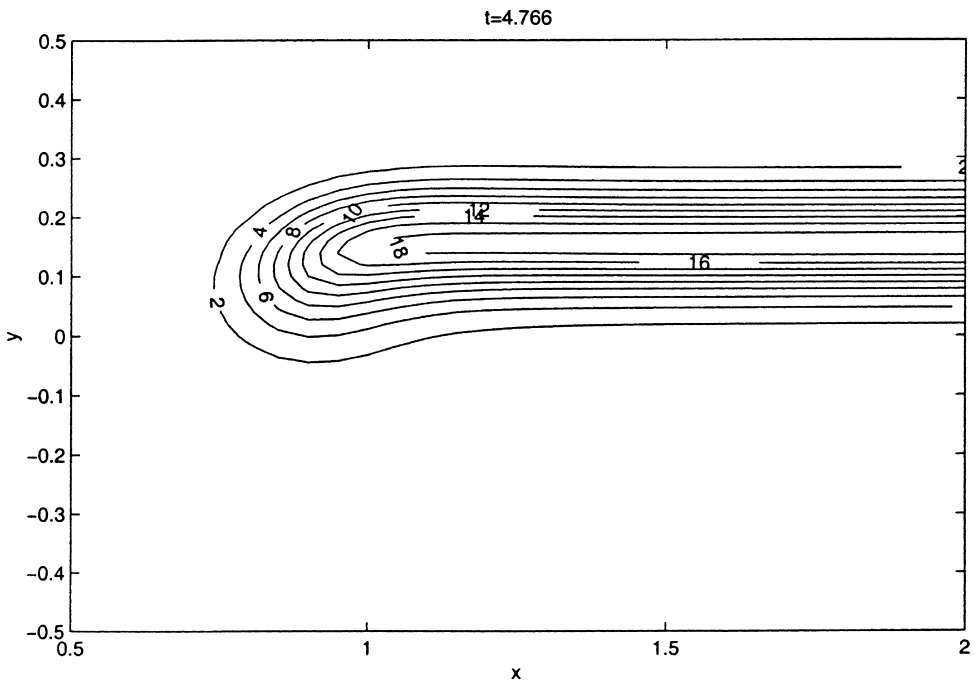

Fig. 44. Edge-flame during the slow retreat phase, from Ref. [70], with permission. Panel notation is that of Ref. [70].

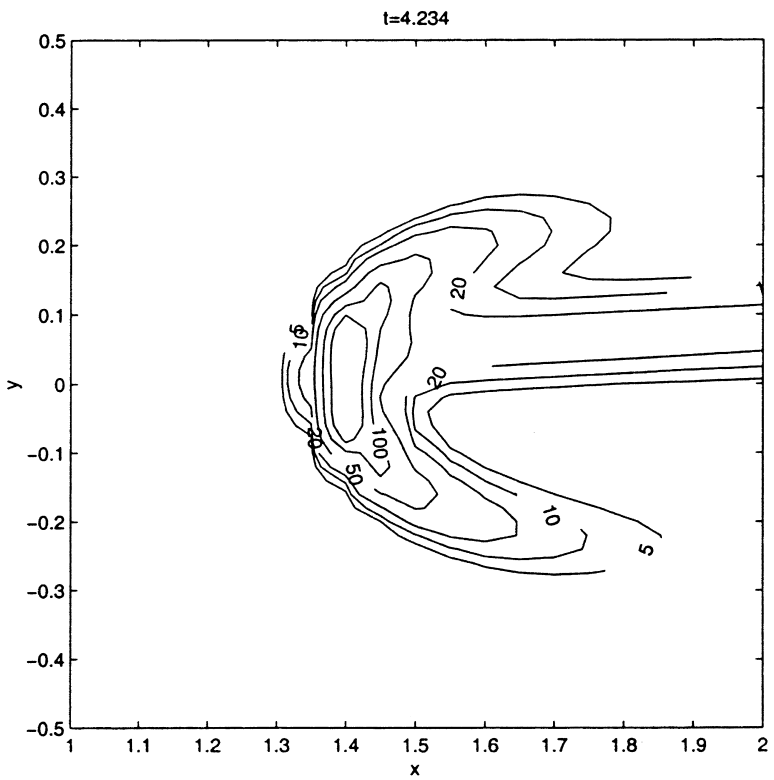

Fig. 45. Edge-flame during the rapid advance phase, from Ref. [70], with permission. Panel notation is that of Ref. [70].

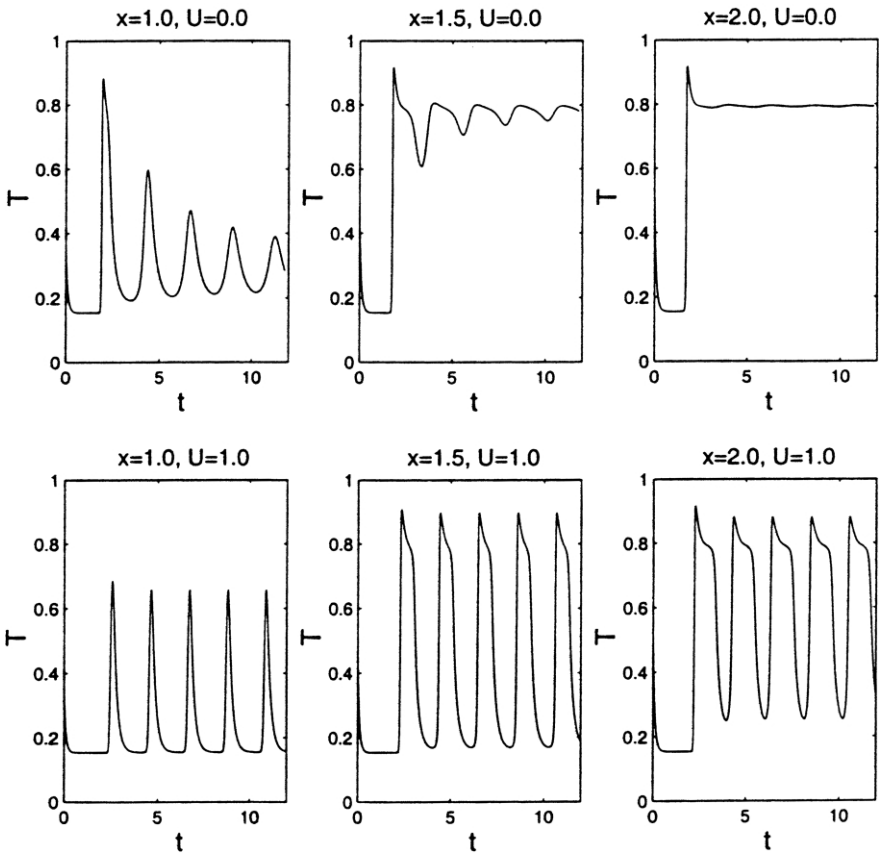

Fig. 46. Destabilization of an edge-flame by an on-edge convective flow. The temperature history at $z = 1.0, 1.5, 2.0$; $x = 0.08$ is shown, $Le_Y = 1.7$, $D = 0.75 \times 10^7$, $U = 0, 1$, from Ref. [71], with permission. Panel notation is that of Ref. [71].

z-direction [71]. A working hypothesis, consistent with the experimental record and with the results that we have just described, is that weakening the flame encourages edge oscillations, whereas strengthening the flame discourages them. A positive V convectively cools the edge without any compensating enhancement in the fuel flux (since there is no fuel supply in $z < 0$) and so is a weakening influence. A negative V, on the other hand, bathes the edge in hot reactants, strengthening it. We expect then, a destabilizing/stabilizing effect according to whether V is positive or negative.

Fig. 46 shows results for which an established stable flame with $V = 0$ is destabilized when V is increased to 1; and Fig. 47 shows a flame that is unstable when $V = 0$ but is stabilized when V is decreased to -1.

Again the Lewis number must be large enough. When $Le_Y = 1.5$, $D = 0.5 \times 10^7$, an increase in V from zero leads to blow-off without any intervening oscillatory stage.

The values of V experienced by an edge-flame vary greatly, depending on the circumstances. In the case of flame-spread over a fuel-bed, where one of the components of V is self-induced, this component is much smaller for a solid bed (slow spread rate) than it is for a liquid. In a gravitational field, V will have a buoyancy-induced component absent in a microgravity environment. When a forced convective flow is applied there will often be a boundary-layer associated with this flow, and the contribution to V then depends on the location of the edge within this boundary layer. Thus whether in reality one sees oscillations driven by the physics implicit in the present model is not dependent merely on the values of Lewis number and Damköhler number.

Moreover, although our discussion has emphasized the importance of the Lewis number, and it is natural to think of the oscillations as Lewis number-induced ($Le > 1$), in the same way that we think of oscillations for large Lewis number deflagrations, e.g. [72], it should be noted that 'large Lewis number oscillations' can be generated for 1D flames, both deflagrations and diffusion-flames, when the Lewis numbers equal 1. The key to the instability is not so much that a Lewis number is different from 1, but rather that the thermal field and an appropriate species field are non-similar, and this can come about via heat losses, which affect only the thermal field. Thus it has been shown theoretically [73,74] and experimentally [75] that heat loss to a burner can destabilize 1D deflagrations even when the Lewis

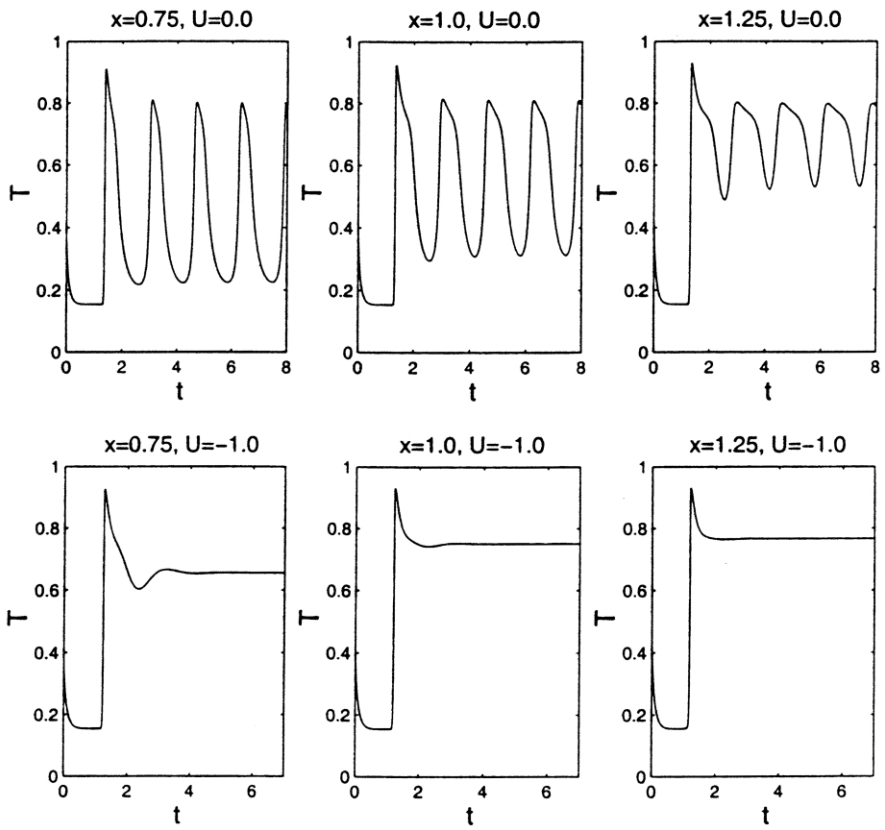

Fig. 47. Stabilization of an edge-flame by an off-edge convective flow. The temperature history at $z = 1.0$, 1.5, 2.0; $x = 0.08$ is shown, $Le_Y = 1.8$, $D = 10^7$, $U = 0$, -1, from Ref. [71], with permission. Panel notation is that of Ref. [71].

number of the deficient component of the mixture is 1; and it has been shown theoretically [76] that volumetric heat losses can destabilize a 1D diffusion flame even when the Lewis numbers of both the fuel and oxidizer are equal to 1. By default, the rubric 'large Lewis number instabilities' is typically assumed to encompass these examples. The lesson for edge-flame studies is that it is conceivable that oscillations could be generated even if all relevant Lewis numbers are equal to 1, and, indeed, recent work on a Burke–Schumann configuration with radiation losses (in addition to the losses to the burner rim) provides an example [77].

12.3. Effects of a cold probe

Insertion of a cold probe into the combustion field in the neighborhood of the edge will weaken it; and, bearing in mind the preceding discussion, it will also increase the dissimilarity between the T-field and the Y-field. Thus oscillations are encouraged and, indeed, such an effect was seen during candle-burning experiments on board the Mir space station. To model such a disturbance, we first create a steady 2D combustion field. Then, within a rectangle $[z_1, z_2] \times [x_1, x_2]$, we adjust the temperature at each mesh point (z_i, x_j) according to the formula

$$T_{ij} = T_o + [T_{ij} - T_o]e^{-t/\lambda}. \tag{90}$$

Fig. 48 shows the consequences of this when $Le_Y = 1.7$, $D = 0.75 \times 10^7$, $\lambda = 1$ and the rectangle is $[0,1.5] \times [-0.1,0.1]$. The temperature within the rectangle is significantly reduced by $t \sim 1-2$ and on this scale the flame shrinks from the probe, pulling back a distance 1 or so, a retreat that is complete by $t = 6$. Subsequently ($t > 10$) small oscillations commence, grow, and a limit cycle is established by $t \approx 30$.

13. Ronney's experimental studies

Edge-flames, in both the premixed [34] and non-premixed [78] context, have been studied by Ronney and his coworkers using a slot counterflow apparatus with, literally, a twist, Fig. 49. By misaligning the nozzles by a few degrees, a rate-of-strain gradient is generated across the width of the slot, and the parameters (flow-rate, reactant concentrations, etc.) can be adjusted so that where the nozzle separation is greatest the Damköhler number is greater than the zero edge-speed value D_0, and where the

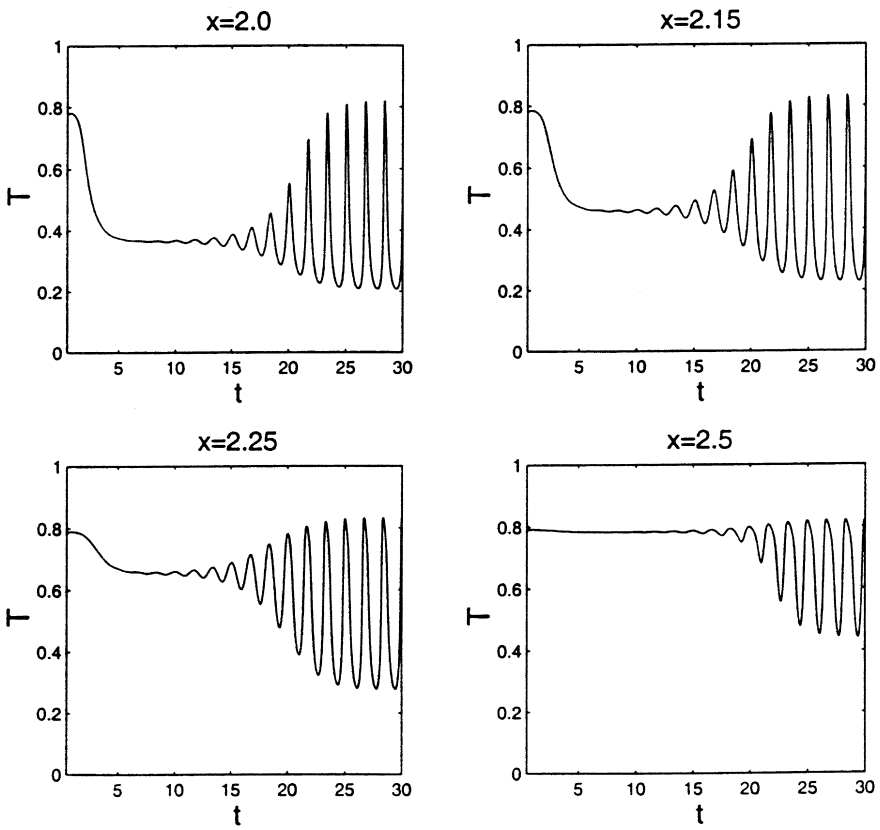

Fig. 48. Destabilizing effect of a heat sink. The temperature history at $z = 2.0, 2.15, 2.25, 2.5$; $x = 0.08$ is shown, sink (cf. Eq. (90) at $[0,1.5] \times [-0.1,0.1]$, from Ref. [71], with permission. Panel notation is that of Ref. [71].

nozzle separation is least the Damköhler number is less than D_0. Consequently, the flame can exist over a fraction of the width only, and an edge-flame is created. If we assume that the gas flow across the width is small, whether generated by the misalignment or by pressure gradients linked to the non-uniform heating, the edge-speed will essentially be zero and the strain at the edge will define the watershed Damköhler number D_0.

If the densities of the two flows are equal, and each efflux is uniform, a *global strain rate* can be defined by the formula

$$\sigma(z) = \frac{V_{\text{upper}} + V_{\text{lower}}}{d(z)} \tag{91}$$

where d is the separation distance, and z is measured across the width. The strain rate will vary through the combustion field of course, due to thermal expansion, and the only apparatus-independent measure is unavailable, as it is defined by cold gases on a scale large compared to the flame thickness, so that Eq. (91) is used by default. The same difficulty arises for aligned nozzles.

Typical results for non-premixed edge-flames are shown in Fig. 50 for a stream of O_2/He impinging against a stream of C_3H_8/He, with the injection speeds fixed at 10 cm/s. The C_3H_8/O_2 ratio is fixed at 10, and the amount of He diluent is varied to vary the mole percent of fuel. The aligned-jet data points define extinction strain rates for the 1D flame, and so define D_e as a function of fuel concentration. The misaligned-jet data, misalignment-independent in the range 2.86–4.51 degrees, define variations in D_0 for the edge-flame. (These are large Lewis number supplies (3.55 for C_3H_8/He, 1.69 for O_2/He) but no oscillations are observed perhaps because the video parameters do not permit the capture of oscillations greater than 15 Hz.)

Observations for premixed configurations (single flame or twin flame) reveal flame shapes of the kind shown in Figs. 17 and 21. Of the various mixtures examined ($CH_4/O_2/CO_2$ with $Le = 0.6$, CH_4/air with $Le = 0.9$, C_3H_8/air with $Le = 1.7$, C_3H_8/O_2/He with $Le = 3$) only the propane mixtures in the twin-flame configuration show differences between D_e and D_o which are significantly larger than either the scatter or the variations due to misalignment variations. It does not follow, however, that edge-flame extinction will only occur for local strain comparable to the 1D quenching value. Once an edge is created in a region of high strain it can be carried as a failure wave into a region of lower strain by a sufficiently strong gas flow parallel to the sheet. Undoubtedly this is what is happening in the sublimit configuration of Fig. 1e.

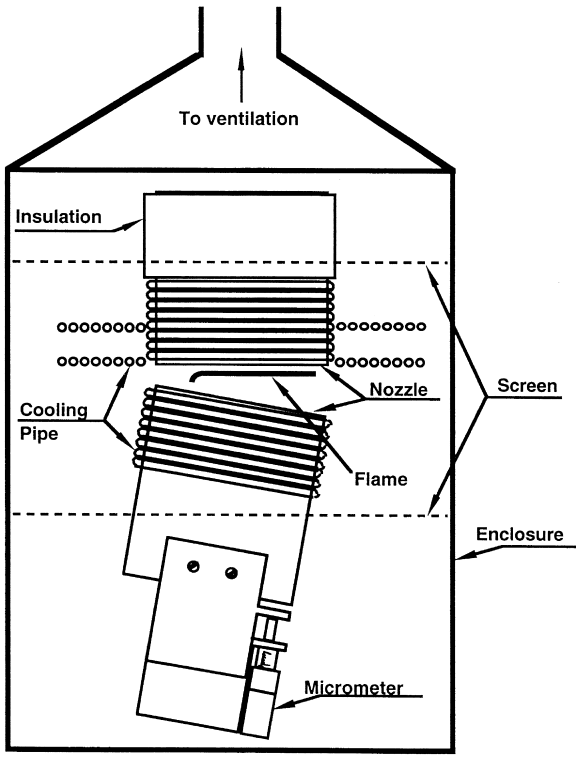

Fig. 49. The edge-flame experimental apparatus of Ronney, from Ref. [34], with permission.

For $CH_4/O_2/CO_2$ mixtures, twin flames, cellular structures are observed at small strain, but not at large strain, which is consistent with the observation in Ref. [48] that sublimit structures exist for $Le = 0.5$, but not for $Le = 0.7$. For the same mixture, single-flame cellular structures are seen for all non-extinguishing strains, probably a consequence of heat loss to the inert stream, as it is known that heat losses encourage the cellular instability [79].

Fig. 32 is typical of the sublimit structures (here a single string and a double string) observed in the experimental study at low Le, both for premixed and non-premixed configurations.

14. Oscillating premixed edge-flames

Consider a narrow deep slot of width $2L$ through whose opposite faces a combustible mixture is injected, with speed v_0 (>0). The gases travel towards the open end of the slot, and their motion creates a plane straining flow, defined when the gas density is constant by the rotational Proudman–Culick solution [80,81]

$$\frac{v}{v_0} = -\sin\left(\frac{\pi}{2}\frac{y}{L}\right), \qquad \frac{u}{v_0} = \frac{\pi}{2L}x\cos\left(\frac{\pi}{2}\frac{y}{L}\right), \tag{92}$$

where x is measured along the slot axis, y is measured perpendicular to the axis, and (u, v) are the velocity components. (Note that this is the constant density solution relevant to the plane counterflow between two nozzles with plug flow conditions at the nozzle exit planes).

This configuration has been studied experimentally [82] in the context of HMX propellants (then the injection is associated with pyrolysis of the propellant), and has been modeled numerically [83]. In both cases, twin deflagrations can be supported with some kind of edge structure near the closed end of the slot. In certain circumstances, the experiments reveal an oscillating instability (advancing and retreating edge), and the numerical work [83] pursues the hypothesis that this is a Lewis number effect, as for the non-premixed edge oscillations that we described earlier. And indeed, oscillations are reported only for sufficiently large

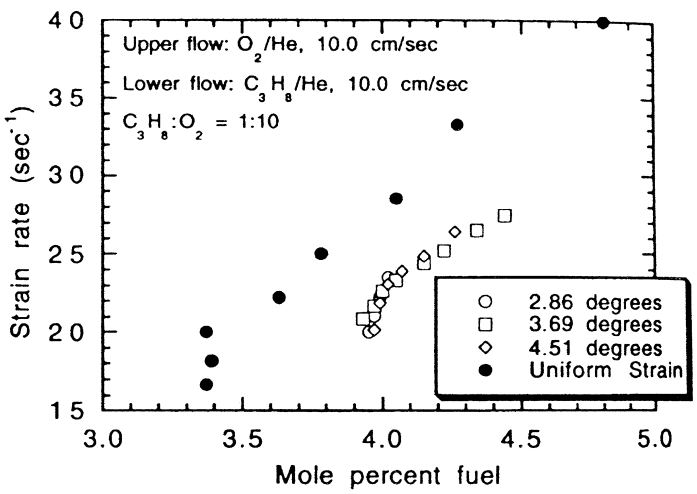

Fig. 50. Experimental data for a counterflow of oxygen/helium with propane/helium, from Ref. [78], with permission. Filled points, D_e; open points, D_0 for various misalignment angles.

Lewis numbers, and for Damköhler numbers (controlled by the rate of strain v_0/L) close to the limit (extinction) value.

15. Edge-flames and turbulence

Non-premixed turbulent combustion is an important subject, long studied. Although much of the burning occurs within diffusion flames, or flamelets, local destruction of a flamelet leads to reactant mixing, and the mixture generated can, in due course, be ignited. The earlier discussion of holes in diffusion flames is relevant if one pictures a distorted wrinkled diffusion flame in which holes are torn when the local scalar dissipation rate $\chi = 2\mathscr{D}|\nabla Z|^2_{\text{stoich.}}$ exceeds the quenching value χ_e, but heal by inward propagation of the edge when χ, a stochastic variable, subsequently drops below χ_0 or thereabouts, depending on the size of the hole.[6] Lifted flames have long been studied as a framework in which it is hoped that important insights into the physics of non-premixed combustion can be achieved.

At its simplest level, the problem of a lifted flame is the determination of where and how the flame-base is stabilized, as for laminar lifted flames. But the turbulent problem is much more difficult because of the difficulty of identifying the ingredients which affect the speed of the flame-base (edge), and of determining their quantitative impact.

There are two old theories of lifted turbulent flames, both advanced before the concept of edge-flames was established, and before modern diagnostic tools were developed which permit a detailed determination of the combustion field in the neighborhood of the base.

The earliest is the proposal by Vanquickenborne and van Tiggelen [84] that full mixing at the molecular level occurs upstream of the flame base, which is, accordingly, a deflagration that travels at the turbulent flame-speed, one significantly greater than the laminar flame-speed S_o.

In contrast, Peters [5] focuses on the diffusion flame that trails downstream of the flame base and argues that upstream of the base the flame cannot exist, whereas downstream it can. From this point of view, χ_e plays an important role. The mean value of χ first increases with distance from the burner as the turbulent intensity grows, and then decreases because of dissipation, and it is argued that the flame base is stabilized in this second region. The precise location is defined by the idea that upstream of the base χ is greater than χ_e often enough and in a large enough fraction of the combustion field that the diffusion flame cannot survive.

As we noted, both theories were proposed before the concept of edge-flames was established. We can link the deflagration concept of Ref. [84] to edge-flames by supposing that the deflagration comprises the two branches of a large Damköhler number tribrachial flame, branches that are subject to stretch and to wrinkling.

On the other hand, trying to place the second theory [5] in the edge-flame context immediately presents difficulties. Propagation is an essential characteristic of an edge-flame, and yet this plays no role in the theory. Moreover, when $\chi \sim \chi_e$ the edge-speed is negative and yet the flame-base must, on average, have a positive speed relative to the fluid: thus χ_0 would seem more to the point than χ_e.

Both theories, by focusing on the extremes, highlight the duality of edge-flames. If one thinks of stretch effects (relevant to deflagrations) and scalar dissipation effects (relevant to diffusion flames) in steady laminar flames of the kind that we have examined, both can be related to a single parameter, the Damköhler number. But in unsteady flows, such as turbulent flows, this simple connection is broken: the local instantaneous stretch is defined by local velocity gradients and flame curvature; the scalar dissipation rate is defined by the instantaneous balance of the various terms in the equation for the scalar Z. The theory of Ref. [84] thinks of the edge-flame purely in terms of its deflagration structures; the theory of Ref. [5] thinks of the edge-flame purely in terms of its trailing diffusion flame.

As also we noted earlier, these early theories were advanced before the development of modern diagnostic methods, and these have now provided crucial insights. For example, the scalar dissipation rate near the flame-base is much smaller than χ_e [85] and for this, and other reasons, there is now a consensus that the scalar dissipation theory is not correct [86], an unfortunate example of a charming theory undone by the facts.

Although the gas speed at the mean flame-base position can be as large as $25S_o$, the gas speed at the instantaneous position is no more than $3S_o$ [87]; moreover, a co-flow greater than $3S_o$ causes flame blowoff. And although mixing is complete upstream of the base, the mixture conditions at the base do not correspond to the maximum flame-speed [88]. These observations are not consistent with the turbulent deflagration theory.

Indeed, it would appear that the flame base is essentially a laminar edge-flame, albeit one influenced by a number of ingredients absent in a laminar flow field. Thus Muñiz and Mungal [89] established that the velocity field near the base is comparable in structure and magnitude to what one would expect from the laminar calculations of Ref. [41]. What precisely stabilizes the edge is uncertain however, as there are a number of ingredients that could affect the speed. The list includes stretch, curvature, the scalar dissipation rate, mixture-strength intermittancy, and transport of burnt gases ahead of the edge via large scale eddies. A rational description that could account for all of these effects in a quantitatively accurate fashion seems unlikely.

What can be done, of course, is an investigation of some of these ingredients in other contexts. Thus Refs. [90,91] use a numerical strategy to examine what happens when an edge-flame, initially exhibiting a strong tribrachial structure,

[6] In the general context, χ plays the role that the rate of strain α plays for laminar counterflow flames, and so the Damköhler number $\sim 1/\chi$.

propagates between twin counter-rotating vortices, which generate an unsteady non-uniform flow field. In Ref. [91] the edge-speed relative to the fluid is shown to correlate with a locally calculated Karlovitz number, but not with the scalar dissipation rate.

16. Edge-flame holding

Sections 8 and 15 have something to say about flame-holding, but only in local gradients. Of a different nature is holding near walls. Fuel and oxidizer streams separated by an infinitesimally thick, semi-infinite splitter plate define a configuration of some importance, one that is discussed in Ref. [92].

Let us first consider the flow sans combustion. Upstream of the plate edge there are Blasius boundary layers in which the two flows satisfy the no-slip condition at the plate. The jump in boundary conditions at the plate edge creates a wake in which the gas speed along and in the neighborhood of the detachment streamline increases with distance (z) as the velocity field more and more resembles the similarity solution for a shear layer. When the Reynolds number based on a length comparable to the two boundary layer thicknesses at the plate edge is large, the evolution of the wake has well-defined structural components. Most notably, there is a triple-deck structure in the neighborhood of the edge, and this transitions to a Goldstein wake. In the inner region of the Goldstein wake, the streamwise velocity grows like $x^{1/3}$. Both in the triple deck and the Goldstein wake streamwise diffusion is negligible, and for subsonic flow an upstream influence is generated only because the external inviscid flow field is displaced via the displacement thickness, a quantity that is a decreasing function of z behind the plate edge. (In supersonic flows, discussed in a combustion context by Jackson [93], there is no upstream influence at all.)

On a much smaller scale than that of the triple-deck there is a Navier–Stokes region at the very edge itself. This is usually ignored, since the triple deck can be discussed independently, but in a combustion context it is precisely the region where a flame edge will be located that can lose heat to the plate. Should the flame edge move out of the Navier–Stokes region into the triple deck or Goldstein wake, it will be controlled by local gradients in these regions, and not the plate.

Following ignition and the establishment of a flame, the flow field that we have described will be modified, but the broad details still provide a meaningful framework within which to discuss the combustion field.

It is helpful (but not necessary) to discuss the results of Liñán [92] in the context of the 1D model, and for this purpose we will examine Eq. (24) but with V replaced by Cs^{γ} $(0 < \gamma < 1)$, an accelerating flow, and with the boundary condition $T = T_w$ at $s = 0$. Not surprisingly, in

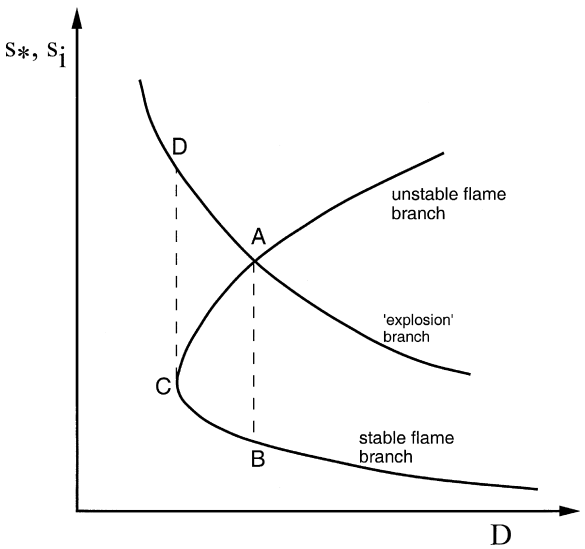

Fig. 51. Solution branches for a non-premixed flame held behind a thin splitter plate.

view of the earlier discussion, the choice $D = O(1/\varepsilon^3)$ leads to relevant solutions (discussed in Ref. [94] when $\gamma = 1$.) On this scale, there is a turning point in the D–s_* plane (s_* is the reaction zone location) with no solutions for D less than some minimum (blow-off) and two solution branches for D greater than this minimum, Fig. 51. On the lower branch, s_* is a decreasing function of D, and this corresponds to stable physically realizable solutions; the upper branch corresponds to unstable solutions.

The mathematical description far along the upper branch can be uncovered by writing

$$s = s_* + \frac{1}{s_*^{\gamma}}\xi, \quad s_* \to \infty, \tag{93}$$

whence Eq. (24) becomes

$$C\frac{\mathrm{d}\theta}{\mathrm{d}\xi} - \frac{\mathrm{d}^2\theta}{\mathrm{d}\xi^2} = \frac{D(1-\theta)^2}{s_*^{2\gamma}}\exp\frac{1}{\varepsilon}\left(1 - \frac{1}{\theta}\right) \tag{94}$$

where $\theta \to \theta_w$ as $\xi \to -\infty$. This problem is that of the classical deflagration, and the instability here is merely the static one: A shift of the flame downstream does not change its speed but places it in a faster stream and so it is swept away; a shift of the flame upstream places it in a slower stream, and so it flashes back towards the plate. The usual flame analysis for the stationary solution shows that

$$s_* \sim (\varepsilon^3 D)^{1/2\gamma} \tag{95}$$

(and so D must be large).

There is a third solution branch which can be called the explosion branch as physically it corresponds to the homogeneous explosion of the mixture as it is convected

downstream, and is described by the equation

$$Cs^{\gamma}\frac{\mathrm{d}\theta}{\mathrm{d}s} = D(1-\theta)^2 \exp\frac{1}{\varepsilon}\left(1-\frac{1}{\theta}\right). \tag{96}$$

In the proper 2D context this was first discussed in Ref. [95], where for the first time can be found a theoretical discussion of a flame structure with the premixed and diffusion flame branches that we now associate with flames in mixing layers. This is not a tribrachial flame in the sense of this review, however, as it does not have a well-defined propagation speed, and any movement that it might display corresponds only to the locus of the ignition point.

To identify the ignition point s_{i} from Eq. (96) we follow Frank-Kamenetskii's familiar strategy and write

$$\theta = \theta_{\mathrm{w}}(1+\varepsilon\theta_{\mathrm{w}}\phi), \qquad s^{1-\gamma} = \frac{\tau}{B},$$
$$B = \frac{D(1-\theta_{\mathrm{w}})^2 \exp\frac{1}{\varepsilon}\left(1-\frac{1}{\theta_{\mathrm{w}}}\right)}{\varepsilon\theta_{\mathrm{w}}^2 C(1-\gamma)}, \tag{97}$$

whence

$$\frac{\mathrm{d}\phi}{\mathrm{d}\tau} = \mathrm{e}^{\phi} \tag{98}$$

with blow-up at $\tau = 1$ so that

$$s_{\mathrm{i}} = B^{-1/(1-\gamma)}, \tag{99}$$

a decreasing function of D (Fig. 51). s_{i} is large and the diffusion term justifiably neglected when B is small.

The explosion branch and the upper flame branch cross where s_* from Eq. (95) equals s_{i}, i.e.

$$D \sim \varepsilon^{(5\gamma-3)/(1+\gamma)} \exp\frac{1}{\varepsilon}\frac{2\gamma}{1+\gamma}\left(-1+\frac{1}{\theta_{\mathrm{w}}}\right) \tag{100}$$

when only the dependence on ε is explicitly identified. For sufficiently small ε it is sufficient to look at the exponential dependence and conclude that D is large and B is small, as required.

Consider Fig. 51. Its significance is that, in principle, for arbitrarily small D there is always an explosion solution with the structure described in Ref. [95]. As D is increased, the ignition point moves towards the plate until the cross-over point A is reached. Then a propagating tribrachial flame is generated which is either swept away or propagates upstream until it reaches the position corresponding to B. A subsequent decrease in D moves the solution along the lower flame branch until blow-off occurs at C and an explosion solution is reinstated at D.

There are clearly many ways in which this discussion could be enlarged. It is noted in Ref. [93], for example, that finite plate thickness effects can be important, an idea that is pursued in the low Mach number context in Ref. [96].

17. A note on vocabulary

Contrary to the opinions of the occasional desk editor, the matter of vocabulary is often a matter of personal taste, although poor taste can lead to confusion. To use 'compressible' as a synonym for 'variable density' is no longer a lexicographal error, since so many do it, but it is certainly not helpful to those who wish to know if finite Mach number effects are accounted for or not. I have exercised certain personal choices in this review.

I have used 'inflammable' (rather than 'flammable') since it is the word that I grew up with, and is still widely used outside of the combustion community, albeit less so than, say, 10 years ago. It is with some alarm that I notice that Stephen Pyne, in one of his fascinating books on natural fires, and the way they have shaped the world and us, uses (at least once) inflammable to mean that which cannot burn. Apparently the word runs the risk of becoming a Janus word, like sanction, one that can mean both one thing and its opposite. Perhaps we need to occasionally acknowledge that here the 'in' has no connection with negation.

What I call tribrachial flames are often called triple flames. But 'tribrachial' can be found in the Oxford Dictionary, and gives more sense of the morphology. For those unaccustomed to reading in the life sciences however, it can appear cumbersome. That aside, to use either label for edge-flames without triple structures is silly.

Indeed, that is why the rubric 'edge-flame' was coined. It is more general than 'leading-edge-flame' as edge-flames sometimes follow. And it surely means something quite different than a flame-edge. The distinction is as between a forest-edge—merely the place where the trees end—and an edge-forest, an ecotone with its own distinct biodiversity. But *chacun á son gout*.

18. Concluding remarks

Flame-theory is an old subject with important roots in the 1928 work of Burke and Schumann on diffusion flames, followed some dozen years later by the work of Darrieus, Landau, Frank-Kamenetskii and Zeldovich on deflagrations. A vast literature has emerged in the past 40 years. And so it is remarkable that edge-flames have only been identified and come to be reasonably well understood in the past dozen years, for they are as fundamental and well-defined as the 1D structures that have been the bread and butter of textbooks for decades.

Their roots probably lie in the 1980s when Peters was writing of holes in diffusion flames [5] but as late as 1989 the triple-flame discussion by Dold [25], which looks over its shoulder at the 1965 experimental report of Phillips [24], seems merely a perturbation of the 1D deflagration. And there is no evidence that this author is aware of that the triple ignition structure described by Liñán and Crespo in 1976

[95] was seen by anyone as a pathological version of a propagating flame structure of universal significance, although as we noted earlier, deRis recognized in his 1968 thesis [68] that the edge of a flame traveling over a fuel-bed will have a branched structure.

Indeed, it is not until 1991, with the work of Dold and his colleagues [29,30] that the essential nature of edge-flames begins to emerge, and 1993 when the numerical work of [17] makes this emergence apparent to those for whom asymptotic treatments are not transparent. The linking of edge-speeds (particularly negative ones) to well-known results in 1D reactive systems [21,22], and the recognition that edge-flames have their roots in multivalued 1D responses [32,33], and not just mixing layers, completed our conceptual understanding.

The subsequent literature has been concerned with questions that have their counterparts in classical deflagration and diffusion flame studies—stability, the effects of boundaries, heat losses, flow field gradients, unsteady disturbances, etc. Undoubtedly, the latter efforts will continue, particularly in a context that will improve our understanding of turbulent flames. Also, since in principle there are multi-valued 1D responses more complex than those examined so far, it is possible that new edge-flame structures will be identified in the future.

Acknowledgements

This work was supported by the Air Force Office of Scientific Research, and by the NASA-Glenn Research Center at LewisField.

References

[1] Ross HD. Ignition of and flame spread over laboratory-scale pools of pure liquid fuels. Prog Energy Combust Sci 1994;20:17–63.
[2] Dietrich DL, Ross HD, Frate DT, T'ien JS, Shu Y. Candle flames in microgravity. NASA Conference Publication 10194. Fourth International Microgravity Combustion Workshop; 1997. p. 237–42.
[3] Price EW. Effect of multidimensional flamelets in composite propellant combustion. J Propulsion Power 1995;11(4):717–28.
[4] Jackson TL, Buckmaster J. Heterogeneous propellant combustion. AIAA J 2002;40(6):1122–30.
[5] Peters N, Williams FA. Liftoff characteristics of turbulent jet diffusion flames. AIAA J 1983;21(3):423–9.
[6] Jarosinski J, Strehlow RA, Azarbarzin A. The mechanisms of lean limit extinguishment of an upward and downward propagating flame in a standard flammability tube. Proc Combust Inst 1982;19:1549–57.
[7] Hegde U, Bahadori MY, Stocker DP. Temporal instability and extinction of a microgravity jet diffusion flame. AIAA paper 99-0582. 37th AIAA Aerospace Sciences Meeting and Exhibit; 1999.
[8] Brahmi L, Vietoris T, Joulain P, David L, Torero J. The effects of parietal fuel injection on the geometry of a low velocity laminar diffusion flame. AIAA Paper 99-0581. 37th AIAA Aerospace Sciences Meeting and Exhibit; 1999.
[9] Kodama H, Miyasaka K, Fernandez-Pello AC. Extinction and stabilization of a diffusion flame on a flat combustible surface with emphasis on thermal controlling mechanisms. Combust Sci Technol 1987;54:37–50.
[10] Chen C-H, T'ien JS. Diffusion flame stabilization at the leading edge of a fuel plate. Combust Sci Technol 1986;50:283–306.
[11] Markstein GH. Nonsteady flame propagation. AGARDograph No. 75, New York: MacMillan; 1964.
[12] Pelcé P, Clavin P. Influence of hydrodynamics and diffusion upon the stability limits of laminar premixed flames. J Fluid Mech 1982;124:219–37.
[13] Matalon M, Matkowsky B. Flames as gasdynamic discontinuities. J Fluid Mech 1983;124:239–59.
[14] Lewis B, von Elbe G. Combustion, flames and explosions of gases, 2nd ed. New York: Academic Press; 1961. section V.4.
[15] Hassan MI, Aung TA, Faeth GM. Measured and predicted properties of laminar premixed methane/air flames at various pressures. Combust Flame 1998;115:539–50.
[16] Liñán A. The asymptotic structure of counterflow diffusion flames for large activation energies. Acta Astronaut 1974;1:1007–39.
[17] Kioni PN, Rogg B, Bray KNC, Liñán A. Flame spread in laminar mixing layers: the triple flame. Combust Flame 1993;95:276–90.
[18] Echekki T, Chen J. Structure and propagation of methanol–air triple flames. Combust Flame 1997;114:231–45.
[19] Kioni P, Bray K, Greenhalgh D, Rogg B. Experimental and numerical studies of a triple flame. Combust Flame 1999;116:192–206.
[20] Weber RO, Mercer GN, Gray BF, Watt SD. Combustion waves: non-adiabatic. In: Buckmaster J, Takeno T, editors. Modeling in combustion science. Lecture notes in physics 449, Berlin: Springer; 1995. p. 285–95.
[21] Buckmaster J. Edge-flames. J Engng Math 1997;31:269–84.
[22] Buckmaster J. Edge-flames and their stability. Combust Sci Technol 1996;115:41–68.
[23] Grindrod P. Patterns and waves. Oxford: Clarendon Press; 1991.
[24] Phillips H. Flame in a buoyant methane layer. Proc Combust Inst 1965;10:1277–83.
[25] Dold JW. Flame propagation in a non-uniform mixture: analysis of a slowly-varying triple-flame. Combust Flame 1989;76:71–88.
[26] Buckmaster J. The structure and stability of laminar flames. Annu Rev Fluid Mech 1993;25:21–53.
[27] Buckmaster J, Matalon M. Anomalous Lewis number effects in tribrachial flames. Proc Combust Inst 1988;22:1527–35.
[28] Daou J, Liñán A. The role of unequal diffusivities in ignition and extinction fronts in strained mixing layers. Combust Theor Model 1998;2(4):449–77.
[29] Hartley LJ, Dold JW. Flame propagation in a nonuniform mixture: analysis of a propagating triple-flame. Combust Sci Technol 1991;80:23–46.
[30] Dold JW, Hartley LJ, Green D. Dynamics of laminar triple-flamelet structures. In: Fife PC, Liñán A, Williams F, editors. Dynamical issues in combustion theory. The IMA volumes in

mathematics and its applications, vol. 35. Berlin: Springer; 1991. p. 83–105.
[31] Ghosal S, Vervisch L. Theoretical and numerical study of a symmetric triple flame using the parabolic flame path approximation. J Fluid Mech 2000;415:227–60.
[32] Buckmaster J. Proceedings of the 16th International Colloquium on the Dynamics of Explosions and Reactive Systems. Wydawnictwo Akapit, Krakow; 1997. p. 124–7 and 132–5.
[33] Vedarajan TG, Buckmaster J. Edge-flames in homogeneous mixtures. Combust Flame 1998;114:267–73.
[34] Liu J-B, Ronney PD. Premixed edge-flames in spatially varying straining flows. Combust Sci Technol 1999;144: 21–45.
[35] Vedarajan G, Buckmaster J, Ronney P. Two-dimensional failure waves and ignition fronts in premixed combustion. Proc Combust Inst 1998;27:537–44.
[36] Savas Ö, Gollahalli SR. Stability of lifted round gas jet flame. J Fluid Mech 1986;165:297–318.
[37] Chung SH, Lee BJ. On the characteristics of laminar lifted flames in a nonpremixed jet. Combust Flame 1991;86:62–72.
[38] Lee BJ, Chung SH. Stabilization of lifted tribrachial flames in a laminar nonpremixed jet. Combust Flame 1997;109: 163–72.
[39] Lee BJ, Cha MS, Chung SH. Characteristics of laminar lifted flames in a partially premixed jet. Combust Sci Technol 1997; 127:55–70.
[40] Ko YS, Chung SH, Kim GS, Kim SW. Stoichiometry at the leading edge of a tribrachial flame in laminar jets from Raman scattering technique. Combust Flame 2000;123:430–3.
[41] Ruetsch GR, Vervisch L, Liñán A. Effect of heat release on triple flames. Phys Fluids 1995;7:1447–54.
[42] Ghosal S, Vervisch L. Stability diagram for lift-off and blowout of a round jet laminar diffusion flame. Combust Flame 2001;124:646–55.
[43] Plessing T, Terhoeven P, Peters N, Mansour MS. An experimental and numerical study of a laminar triple flame. Combust Flame 1998;115:335–53.
[44] Nagayam V, Balasubramanian R, Ronney PD. Diffusion flame-holes. Combust Theor Model 1999;3:727–42.
[45] Buckmaster J, Jackson TL. Holes in flames, flame isolas, and flame edges. Proc Combust Inst 2000;28:1957–64.
[46] Pellet G, Isaac K, Humphreys Jr. W, Gartrell L, Roberts W, Dancey C, Northam G. Velocity and thermal structure and strain-induced extinction of 14 to 100% hydrogen–air counterflow diffusion flames. Combust Flame 1998;112: 575–92.
[47] Lee J, Frouzakis C, Boulouchos K. Two-dimensional direct numerical simulation of opposed-jet hydrogen/air flames: transition from a diffusion to an edge flame. Proc Combust Inst 2000;28:801–6.
[48] Buckmaster J, Short M. Cellular instabilities, sublimit structures and edge-flames in premixed counterflows. Combust Theor Model 1999;3:199–214.
[49] Daou J, Liñán A. Ignition and extinction fronts in counterflowing premixed reactive gases. Combust Flame 1999;118: 479–88.
[50] Ronney P. Near-limit flame structures at low Lewis number. Combust Flame 1990;82:1–14.
[51] Buckmaster J, Smooke M, Giovangigli V. Analytical and numerical modeling of flame-balls in hydrogen–air mixtures. Combust Flame 1993;94:113–24.
[52] Buckmaster J, Joulin G. Flame balls stabilized by suspension in fluid with a steady linear ambient velocity distribution. J Fluid Mech 1991;227:407–27.
[53] Kagan L, Sivashinsky G. Self-fragmentation of nonadiabatic cellular flames. Combust Flame 1997;108:220–6.
[54] Buckmaster J. A flame-string model and its stability. Combust Sci Technol 1992;84:163–76.
[55] Kaiser C, Liu J-B, Ronney P. Diffusive-thermal instability of counterflow flames at low Lewis number. AIAA paper 2000-0576. 38th Aerospace Sciences Meeting and Exhibit; 2000.
[56] Kim JS, Williams FS, Ronney PD. Diffusional-thermal instability of diffusion flames. J Fluid Mech 1996;327: 273–301.
[57] Cheatham S, Matalon M. A general asymptotic theory of diffusion flames with application to cellular instability. J Fluid Mech 2000;414:105–44.
[58] Buckmaster JD, Ludford GSS. Lectures on mathematical combustion. CBMS-NSF regional conference series in applied mathematics, vol. 43. Philadelphia: SIAM Press; 1983.
[59] Thatcher RW, Dold JW. Edges of flames that don't exist: flame-edge dynamics in a non-premixed counterflow. Combust Theor Model 2000;4:435–57.
[60] Kochevets SV. Cellular instability of diffusion flames in the counterflow configuration. MS Thesis, University of Illinois at Urbana-Champaign; 1999.
[61] Short M, Buckmaster J, Kochevets S. Edge-flames and sublimit hydrogen combustion. Combust Flame 2001;125: 893–905.
[62] Kucuck S, Matalon M. The onset of oscillations in diffusion flames. Combust Theor Model 2001;5(2):217–40.
[63] Joulin G. Preferential diffusion and the initiation of lean flames of light fuels. SIAM J Appl Math 1987;47:998–1016.
[64] Goldmeer JS, Urban DL, T'ien JS. Combustion and extinction of PMMA cylinders during depressurization in low-gravity, paper presented at the 1993 Fall Technical Meeting of the Eastern States Section of the Combustion Institute. A published report, sans discussion of the oscillations, can be found in Fire Safety Journal 1999; 32: 61–88.
[65] Kim I, Schiller DN, Sirignano WA. Axisymmetric flame spread over propanol pools in normal and zero gravities. Combust Sci Technol 1998;139:249–75.
[66] Higuera FJ, Garcia-Ybarra PL. Steady and oscillatory flame-spread over liquid fuels. Combust Theor Model 1998;2:43.
[67] Wichman I. Prog Energy Combust Sci 1992;18:553–92.
[68] deRis JN. The spread of a diffusion flame over a combustible surface. PhD thesis, Harvard University; 1968.
[69] Glassman I, Dryer F. Fire Saf J 1981;3:132.
[70] Buckmaster J, Zhang Y. A theory of oscillating edge-flames. Combust Theor Model 1999;3:547–65.
[71] Buckmaster J, Hegab A, Jackson TL. More results on oscillating edge-flames. Phys Fluids 2000;12(6):1592–600.
[72] Pearlman H, Ronney P. Near-limit behavior of high-Lewis number premixed flames in tubes at normal and low gravity. Phys Fluids 1994;6:4009–18.
[73] Margolis SB. Bifurcation phenomena in burner-stabilized premixed flames. Combust Sci Technol 1980;22:143–69.
[74] Buckmaster J. Stability of the porous plug burner flame. SIAM J Appl Math 1983;43:1335–49.
[75] Gorman M, El-Hamdi M, Robbins KA. Chaotic dynamics near the extinction limit of a premixed flame on a porous plug burner. Combust Sci Technol 1994;98:47–56.

[76] Kirkby LL, Schmitz RA. An analytical study of the stability of a laminar diffusion flame. Combust Flame 1966;10:205–20.
[77] Kurdyumov VN, Matalon M. Radiation losses as a driving mechanism for flame oscillations. Proc Combust Inst 2002;29.
[78] Shay M, Ronney P. Nonpremixed edge flames in spatially varying straining flows. Combust Flame 1998;112:171–80.
[79] Joulin G, Clavin P. Linear stability analysis of non-adiabatic flames: diffusional-thermal model. Combust Flame 1979;35: 139–53.
[80] Proudman I. An example of steady laminar flow at large Reynolds number. J Fluid Mech 1961;9:593–602.
[81] Culick FEC. Rotational axisymmetric mean flow and damping of acoustic waves in solid propellant rocket motors. AIAA J 1966;4(8):1462–4.
[82] Berghout HL, Son SF, Asay BW. Convective burning in gaps of PBX9501. Proc Combust Inst 2000;28:911–7.
[83] Liu Y, Short M. A model for edge-flame oscillations in a thin rectangular propellant crack. Combust Theor Model, in press.
[84] Vanquickenborne L, van Tiggelen A. The stabilization mechanism of lifted diffusion flames. Combust Flame 1966; 10:59–69.
[85] Schefar RW, Namazian M, Kelly J. Stabilization of lifted turbulent-jet diffusion flames. Combust Flame 1994;99: 75–86.
[86] Peters N. Turbulent combustion. Cambridge, NY; 2000.
[87] Hasselbrink Jr. EL, Mungal MG. Characteristics of the velocity field near the instantaneous base of lifted non-premixed turbulent jet flames. Proc Combust Inst 2000;27: 867–73.
[88] Tacke E, Geyer D, Hassel EP, Janicka J. A detailed investigation of the stabilization point of lifted turbulent diffusion flames. Proc Combust Inst 2000;27:1157–65.
[89] Muñiz L, Mungal MG. Instantaneous flame-stabilization in lifted-jet diffusion flames. Combust Flame 1997;111:16–31.
[90] Favier V, Vervisch L. Proc Combust Inst 2000;27:1239–45.
[91] Im HG, Chen JH. Effects of flow-strain on triple flame propagation. Combust Flame 2001;126:1384–92.
[92] Liñán A. Ignition and flame spread in laminar mixing layers. In: Buckmaster J, Jackson TL, Kumar A, editors. Combustion in high-speed flows. Boston: Kluwer; 1994. p. 461–76.
[93] Jackson TL. Stability of laminar diffusion flames in compressible mixing layers. In: Hussaini MY, Kumar A, Voigt R, editors. Major research topics in combustion. Berlin: Springer; 1992. p. 131–61.
[94] Buckmaster J, Weber R. Edge-flame holding. Proc Combust Inst 1996;26:1143–9.
[95] Liñán A, Crespo A. An asymptotic analysis of unsteady diffusion flames for large activation energies. Combust Sci Technol 1976;14:95–117.
[96] Higuera FJ, Liñán A. Flow field of a diffusion flame attached to a thick-walled injector between two coflowing reactant streams. J Fluid Mech 1996;329:389–411.